Detection of a Kinetically Competent Compound-I Intermediate in the Vancomycin Biosynthetic Enzyme OxyB

Andy K. L. Nguy[†], Ryan J. Martinie[†,¶], Amanda Cai[†], and Mohammad R. Seyedsayamdost[†,‡,*]

[†]Department of Chemistry, Princeton University, Princeton, NJ 08544, United States

[¶]Department of Chemistry, Hamilton College, Clinton 13323, United States

[‡]Department of Molecular Biology, Princeton University, Princeton, NJ 08544, United States

ABSTRACT: Cytochrome P450 enzymes are abundantly encoded in microbial genomes. Their reactions have two general outcomes, one involving oxygen insertion via a canonical 'oxygen rebound' mechanism and a second that diverts from this pathway and leads to a wide array of products, notably intramolecular oxidative crosslinks. The antibiotic of-last-resort vancomycin contains three such crosslinks, which are crucial for biological activity and are installed by the P450 enzymes OxyB, OxyA, and OxyC. The mechanisms of these enzymes have remained elusive in part because of the difficulty in spectroscopically capturing transient intermediates. Using stopped-flow UV/Visible absorption and rapid freeze-quench electron paramagnetic resonance spectroscopies, we show that OxyB generates the highly reactive compound-I intermediate, which can react with a model vancomycin peptide substrate in a kinetically competent fashion to generate product. Our results have implications for the mechanism of OxyB and are in line with the notion that oxygen rebound and oxidative crosslinks share early steps in their catalytic cycles.

Nature uses cytochrome P450 enzymes, a superfamily of thiolate-ligated hemoproteins, to achieve stereospecific hydroxylation of inert C-H bonds with bond dissociation energies of ~100 kcal/mol.[1-3] Groves has elucidated the consensus mechanism for this challenging transformation,[4,5] wherein oxygen activation of the ferric heme cofactor yields an iron(IV)oxo porphyrin π-cation radical (cpd-I, Fig. 1A),[6] which abstracts a H-atom from substrate to produce an iron(IV)hydroxide species (cpd-II, Fig. 1A),[7,8] concomitant with formation of a substrate-centered radical. This radical then recombines with the hydroxide of cpd-II, formally known as 'oxygen rebound', to access the alcohol product.[9-11]

Curiously, in many natural product biosynthetic pathways, P450 enzymes do not catalyze oxidations through oxygen rebound.[12-14] Rather, an alternative outcome leads to a variety of intramolecular cyclizations without oxygen insertion. Walsh and Moore have labelled this class 'thwarted oxygenases'.[15] The biosynthetic pathway of vancomycin, the drug of-last-resort against persistent bacterial infections,[16-19] employs three such enzymes, OxyB, OxyA, and OxyC,[20-23] which install distinct aromatic crosslinks (Fig. 1B). Although there have been remarkable advances in our understanding of vancomycin biosynthesis,[24,25] the mechanistic details underlying phenolic crosslink formation, which confers vancomycin its rigid topology and potent activity, remain unknown. In particular, it is unclear whether high-valent iron-oxo species in the P450 catalytic cycle are directly involved.[26-29] Efforts to detect these intermediates have so far been unsuccessful.[30]

To determine if any reactive intermediates could be induced to accumulate under single-turnover conditions with OxyB, we employed the peroxide shunt strategy,[31-33] which circumvents the necessity for enzymatic redox partners to supply reducing equivalents to heme-bound O_2. Instead, the peroxide directly oxidizes ferric heme to the short-lived ferric-hydroperoxo species (cpd-0),[34-36] which subsequently converts to the high-valent iron(oxo) species (Fig. 1A). Rittle and Green conclusively established the existence of cpd-I,[37] which was produced transiently by *m*-chloroperoxybenzoic acid (*m*CPBA) and validated by several spectroscopic methods.

The as-purified OxyB exhibits an intense Soret band near 419 nm and Q-bands at 537 and 570 nm (Fig. 2A), consistent with a low-spin ferric heme resting state. Upon substrate binding, distinctive UV/Vis spectral changes reveal a typical low- to high-spin conversion, characteristic of the so-called type I shift,[38] which allowed us to determine a k_{on} of 9.55 x 10^4 $M^{-1}s^{-1}$ and a K_d of 17 μM between OxyB and its substrate (Figs. 2B, S1, and S2), a 7mer peptide thioesterified to the pantetheine arm of the peptidyl-carrier protein/X (PCP-X)-didomain.[39] Unfortunately, initial peroxide shunt SF-UV/Vis experiments with as-isolated OxyB yielded no spectral changes (Fig. S3). Encouraged by prior reports that P450 activity can be enhanced through further purification by, in particular, removing contaminating fatty acids from the active site,[40] we subjected OxyB to FPLC-based size-exclusion chromatography (Fig. S4). This enriched *holo*-OxyB and resulted in an enhanced Reinheitszahl of ~1.5.

Rapid-mixing of *holo*-OxyB with excess *m*CPBA at 20°C produced a new short-lived intermediate with absorption features around 695 and 363 nm, along with a concomitant decrease in the 419 nm Soret band (Figs. 2C, 2D). A clear set of isosbestic points at 391, 450, 516, and 590 nm indicated only two major species were present in the reaction. The Soret band decayed with biexponential kinetics with the rapid phase beyond the limit of our setup (>300 s^{-1}) and a slow phase of 12.9 s^{-1} associated with an amplitude of 0.43 AU (Fig. 2E). Likewise, the 695 nm feature formed with similar kinetics as the decay of

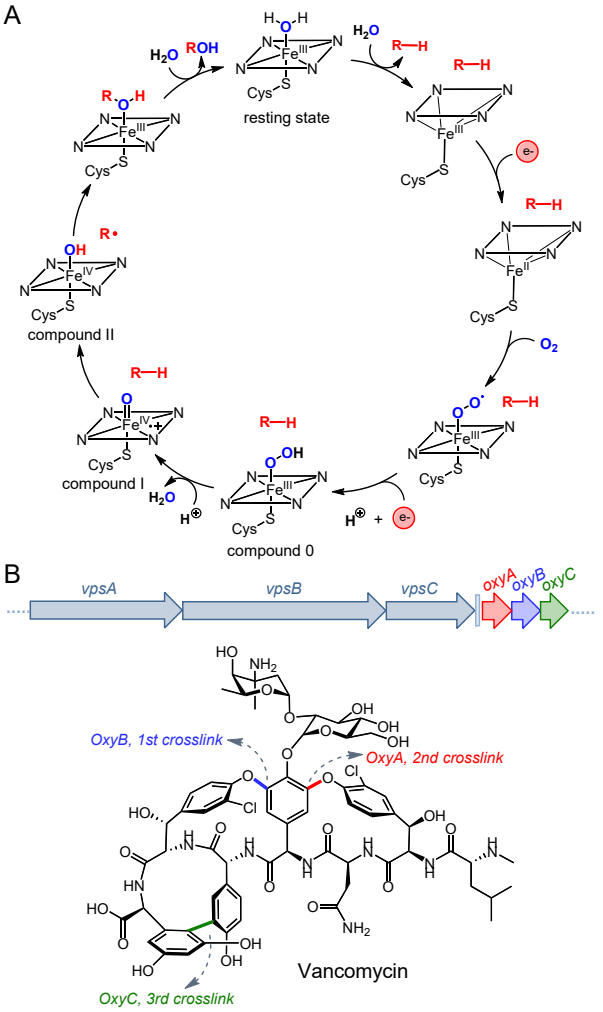

Figure 1. Cytochrome P450 catalytic cycle and abbreviated vancomycin gene cluster. (A) The catalytic cycle for P450s featuring high-valent iron intermediates. (B) Abbreviated vancomycin cluster; shown are three NRPSs and the three P450 enzymes (OxyABC).

the Soret with fast and slow phases of >300 s^{-1} and 14.2 s^{-1} with an amplitude of 0.015 AU (Fig. 2E). The biphasic kinetics may be due to incomplete removal of fatty acids or other ligands or variability in protein quaternary structure. The observed 695 nm feature is reminiscent of the cpd-I intermediate that has been detected in CYP119,[37] APO,[41] and CPO.[42,43] Similar although inconclusive results were reported with CYP121.[44] The putative cpd-I species is present maximally at 70 ms and decays with monoexponential kinetics (2.7 s^{-1}) presumably to the ferric state. However, the complex redox conditions, whereby excess *m*CPBA reoxidizes the heme-cofactor, preclude detection of ferric heme using the Soret band. To better visualize the new absorption feature, the diode array spectrum at 70 ms was subtracted from that at 2 ms, revealing a broad feature with a λ_{max} at 695 nm, diagnostic of cpd-I (Fig. 2F). Given the conversion of ferric heme to cpd-I and its extinction coefficient of ~100 $mM^{-1}cm^{-1}$ (at 419 nm), we calculate an extinction coefficient of ~3,490 $M^{-1}cm^{-1}$ for cpd-I (at 695 nm), indicating that ~43% of the available ferric heme underwent oxidation. Further analyses by singular value decomposition and target testing corroborated the presence of cpd-I (Figs. S5–S7). The former showed two predominant chemical species were present; the abstract spectra associated with these singular values agreed well with those reported for CPO and CYP119.[45] The latter provided an excellent match to the reported target vector for the CYP119 cpd-I.[37] The correlated kinetic changes at 419/695 nm, the blue-shifted Soret upon reaction with *m*CPBA, and the absorbance band at 695 nm all indicate formation of the sought after cpd-I intermediate in OxyB. Analogous SF UV/Vis experiments at 4°C also resulted in cpd-I formation with a ~1.5-fold higher yield and similar spectral features (Fig. S8).

To obtain further evidence for the cpd-I intermediate, we used EPR techniques as an orthogonal spectroscopic method. The X-band EPR spectrum of *holo*-OxyB exhibited low-spin ferric heme features with simulated rhombic *g*-values of 2.45, 2.26, and 1.91 (Fig. 3A).[46] Upon addition of the 7mer-PCP-X substrate, OxyB exhibited a high-spin ferric heme signature (g = 8, 3.64, 1.71), agreeing with the corresponding UV/Vis-based type I shift (Figs. S1, S9). We also observed a novel substrate-dependent low-spin ferric heme species (g = 2.5, 2.25, 1.8),[47-49] consistent with type II binding (Fig. S9). Both these high- and low-spin heme features increased as a function of 7mer-PCP-X concentration (Fig. S10).

From previous studies, the electronic structure of the P450 cpd-I is best described as an S=1 iron(IV)oxo unit exchanged-coupled to an S=½ non-innocent porphyrin radical.[50,51] The resulting system consists of three Kramers doublets, the lowest of which is EPR-active due to strong zero-field splitting arising from the triplet Fe(IV)oxo unit.[52] At temperatures <30 K, cpd-I undergoes fast relaxation due to the double-phonon Orbach relaxation pathway,[53,54] a spin-lattice process facilitated by the higher-lying Kramers doublet. To determine whether OxyB cpd-I can be spectroscopically captured by RFQ-EPR,[55] 0.2 mM of purified *holo*-OxyB was rapidly mixed with 1 mM *m*CPBA at 4°C and the reaction quenched in liquid isopentane maintained at -140 °C after 70 ms. The resulting EPR spectra, recorded as a function of microwave power, revealed a composite signal in agreement with results from CYP119,[37] which also consists of cpd-I and an additional paramagnetic contaminant (Fig. 3B). The spectrum exhibits an axial feature with $g_{\parallel}$=2.03 and $g_{\perp}$=2, alongside a broad up-field spectral tail that is diagnostic for cpd-I.[37,50] Analogous to CYP119, the composite EPR signal increases as a function of power up to 10 mW, consistent with a fast-relaxing cpd-I species.[53,54] This is especially noticeable for the cpd-I upfield spectral tail (Figs. 3B, S11, S12). In contrast to CYP119, disparate power saturation profiles were observed beyond 10 mW for the paramagnetic contaminant(s) at 7 K (Figs. S11-S12).

An RFQ-EPR timecourse from 10–300 ms showed that the composite EPR spectrum increases and decays as a function of time, analogous to the SF-UV/Vis data (Fig. 3C). The ratio of the downfield paramagnetic contaminant to the cpd-I signal varied as a function of time. Spectral deconvolution of the 70 ms signal allowed subtraction of the contaminant, thus revealing the signal for cpd-I (red, Fig. 3D). Spin quantitation gave 58% cpd-I, consistent with the SF-UV/Vis data (Fig. S8). A similar signal, though less intense, was also observed at 10 and 300 ms (Fig. S13). The cpd-I spectrum is consistent with the spin-coupled representation proposed by Debrunner.[50] Specifically, simulation of this signal shows that the π porphyrin radical in the heme normal plane displays a relatively constant, spin-only paramagnetism with $g_{\parallel}^{eff}$ ~2, while the $g_{\perp}^{eff}$ of ~1.995, which resides along the heme plane, is known to be tuned by *J*/*D*, the ratio of spin exchange-coupling to ferryl zero-field splitting (Fig. 3E).[50] A connection between *J*/*D* and a shortened Fe–S distance has been posited,[56,57] suggesting this parameter could

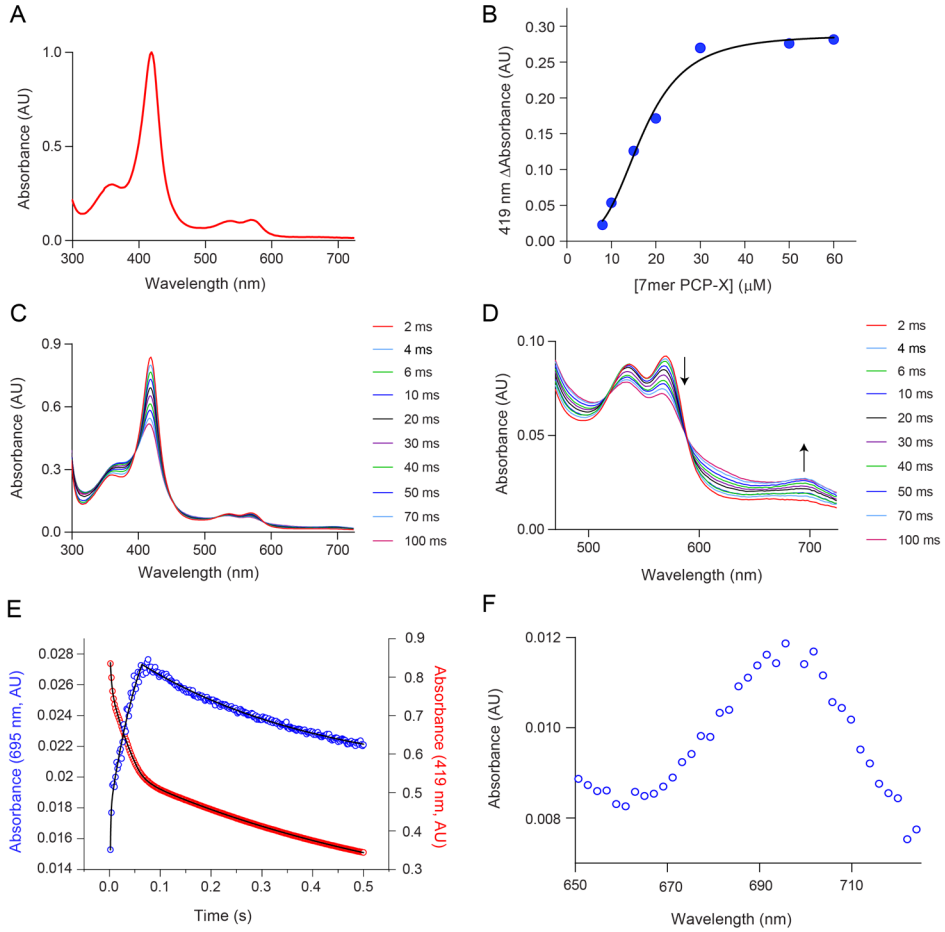

Figure 2. Stopped-flow UV/Vis assessment of the reaction of OxyB with *m*CPBA. (A) UV/Vis spectrum of OxyB. (B) Binding of OxyB to X-PCP-7mer using the type I shift yields k_{on} and K_d of 9.55 x 10^4 M^{-1} s^{-1} and 17 μM, respectively. (C) SF-UV/Vis spectra obtained by rapidly mixing 20 μM ferric *holo*-OxyB with 2 mM *m*CPBA at 20°C. (D) SF-UV/Vis spectra of the Q-band region obtained from panel C. (E) Single-wavelength kinetics upon reaction of OxyB with *m*CPBA. Fits (black lines) describe a double-exponential growth phase and a single-exponential decay phase; see text for fit parameters. (F) UV/Vis difference spectrum for the OxyB cpd-I from panel C.

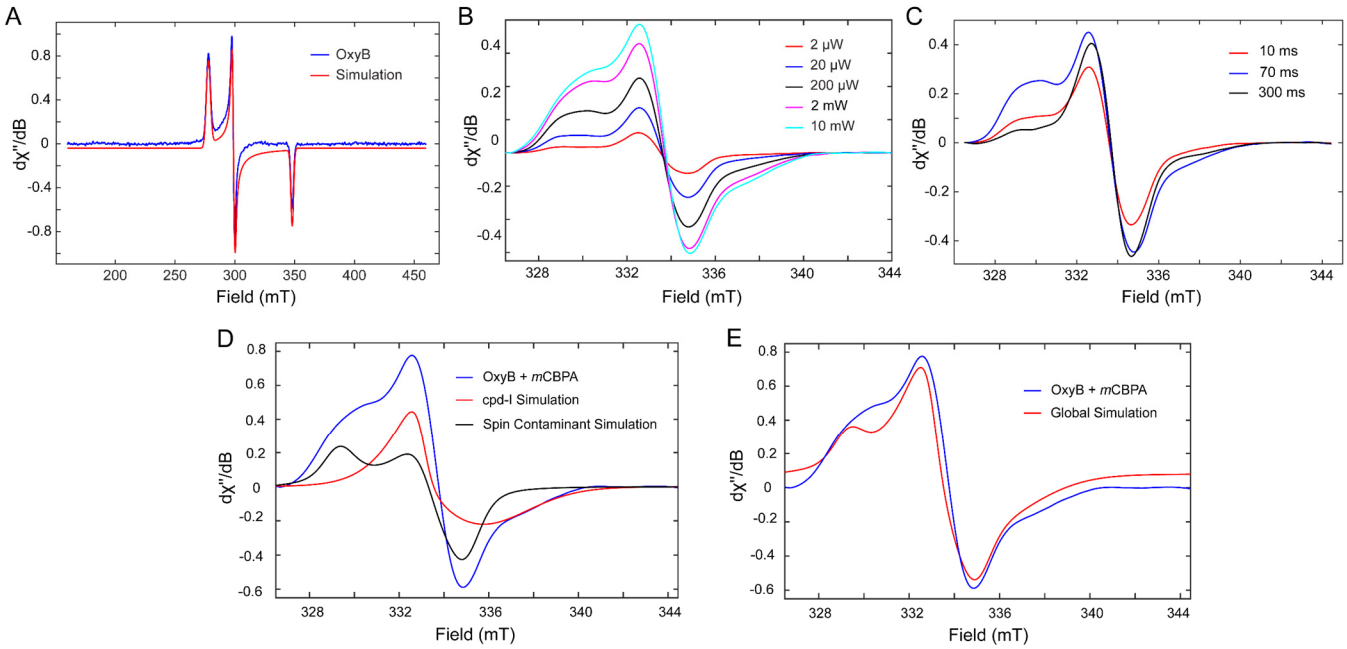

Figure 3. Monitoring the reaction of OxyB with *m*CPBA via RFQ-EPR spectroscopy. (A) X-band EPR spectrum of ferric low-spin OxyB. (B) Composite RFQ-EPR spectra after a 70 ms reaction of OxyB with *m*CPBA as function of microwave power at 10 K. Saturation profiles at 7 K were comparable. (C) Composite RFQ-EPR signals at 10 mW observed as a function of time. (D) Deconvolution of the composite spectrum obtained after a 70 ms reaction (panel C). (E) Global EPR simulation from the summation of OxyB cpd-I and spin contaminant.

be a proxy for cpd-I reactivity. For instance, the *J*/*D* values for CPO,[50] CYP119,[37] and selenocysteine (SeCys)-ligated CYP119[57] are 1.02, 1.30 and 1.43, respectively. In line with this argument, the $g_{\perp}^{eff}$ for the OxyB cpd-I places its *J*/*D* value at ~1.4, in-between CYP119 and SeCys-CYP119.[58] This is noteworthy as the *J*/*D* value suggests that OxyB has intrinsic cpd-I reactivity typical of canonical P450s, although it relies on thwarted oxygenase reactivity to introduce a phenolic crosslink.

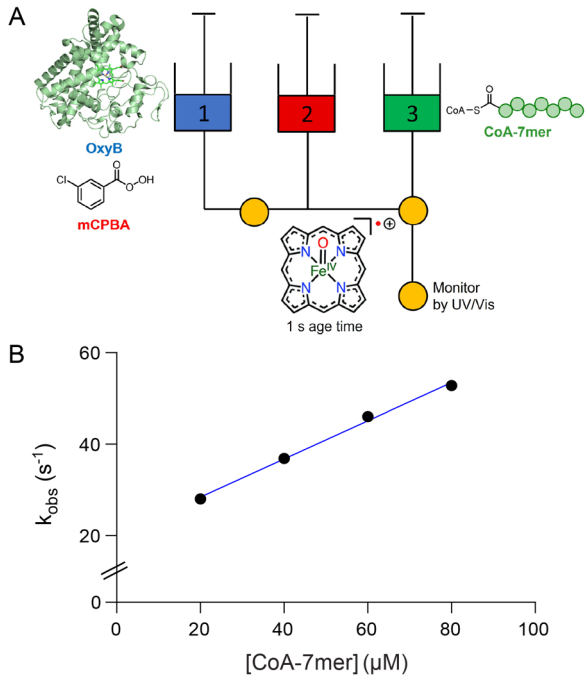

Figure 4. Reaction of OxyB cpd-I with substrate. (A) Sequential SF-UV/Vis schematic, wherein OxyB cpd-I is rapidly formed and then mixed with the 7mer-CoA substrate. (B) Apparent OxyB cpd-I decay rate constants as a function of 7mer-CoA concentration.

Having established cpd-I formation, we next assessed its kinetic competence in reacting with the 7mer-CoA substrate. Sequential mix SF-UV/Vis experiments were conducted in which *holo*-OxyB and *m*CPBA were mixed, held for 1 s to promote formation of cpd-I, and then reacted with 7mer-CoA (Fig. 4A). Determining k_{obs} for consumption of cpd-I as a function of substrate concentration allowed us to derive an apparent second-order rate constant of 4.2 x 10^5 $M^{-1}s^{-1}$ (Figs. 4B, S14), which is similar to those determined for CYP119 against a panel of substrates (10^4–10^7 M^{-1} s^{-1}). Given the OxyB k_{cat} (0.11 s^{-1}) and k_{cat}/K_M (8.3 x 10^3 $M^{-1}s^{-1}$) values,[21] the results indicate that formation and consumption of cpd-I are kinetically competent. Moreover, cpd-I can form in the absence of substrate, a rather surprising result given the highly reactive nature of the intermediate. Finally, immediately after the SF-UV/Vis experiment, the contents of the stop syringe were subjected to HPLC-Qtof-MS analysis and revealed both substrate and the monocyclic product, consistent with cpd-I as the chemically competent intermediate in introducing the first phenolic crosslink in vancomycin (Fig. S15, Tables S1-S2).

Collectively, our findings establish formation of a transient cpd-I intermediate in OxyB, which is kinetically and chemically competent to react with substrate. Thus, the thwarted oxygenase OxyB shares initial steps in the catalytic cycle with canonical P450s. How these enzymes diverge remains to be determined. The presence of multiple aromatic groups in OxyB[59-61] poses several challenges for cpd-I: (1) avoiding oxidation of protein-bound Trp/Tyr residues, and (2) specifically oxidizing Tyr2 among five different phenolic groups within the substrate.[62] The well-documented push-pull effect[63] of heme-thiolates forgoes reduction potential for enhancing the basicity of cpd-II,[64,8] which essentially favors short-range H-atom transfer over long-range orthogonal proton-coupled electron transfer,[65,66] thus addressing the first challenge. Precise positioning of the substrate, guided by the X-domain,[39] could place Tyr2 in contact range of cpd-I, thereby addressing the second challenge, namely, unwanted oxidations in the vancomycin peptide. Consistent with this model are off-site reactions that occur when the X-domain is omitted.[23,62]

ASSOCIATED CONTENT

Supporting Information

Full experimental procedures; additional RFQ-EPR and SF UV/Vis absorption spectra and associated analysis by SVD and target testing; product analysis after rapid reaction of OxyB with substrate. The Supporting Information is available free of charge at:

AUTHOR INFORMATION

Corresponding Author

Mohammad R. Seyedsayamdost – Department of Chemistry and Department of Molecular Biology, Princeton University, New Jersey 08544, *United States;* https://orcid.org/0000-0003-2707-4854;

Email: mrseyed@princeton.edu

Authors

Andy K. L. Nguy – Department of Chemistry, Princeton University, New Jersey 08544, United States; https://orcid.org/0000-0001-8375-3777

Ryan J. Martinie – *Department of Chemistry, Princeton University, New Jersey 08544, United States;* https://orcid.org/0000-0003-1257-2850

Amanda Cai – Department of Chemistry, Princeton University, New Jersey 08544, United States

Present Addresses

¶ Department of Chemistry, Hamilton College, Clinton 13323, United States

Notes

The authors declare no competing financial interest.

ACKNOWLEDGMENTS

We thank Prof. John T. Groves for helpful discussions and the National Institutes of Health (Grant R01 GM129496 to M.R.S.) for financial support. This paper is dedicated to the late memory of C. T. Walsh, whose decades of inquiry into vancomycin resistance and biosynthesis laid the foundation for this work.

REFERENCES

(1) Groves, J. T. Models and Mechanisms of Cytochrome P450 Action. *Cytochrome P450: Structure, Mechanism, and Biochemistry.* **2005**, 1–44.

(2) Denisov, I. G.; Makris, T. M.; Sligar, S. G.; Schlichting, I. *Chem. Rev.* Structure and Chemistry of Cytochrome P450. *Chem. Rev.* **2005**, *105*, 2253–2277.

(3) Ortiz de Montellano, P. R. Hydrocarbon Hydroxylation by Cytochrome P450 Enzymes. *Chem. Rev.* **2010**, *110*, 932 – 948.

(4) Groves, J. T.; McClusky, G A. Aliphatic Hydroxylation via Oxygen Rebound. Oxygen Transfer Catalyzed by Iron. *J. Am. Chem. Soc.* **1976**, *98*, 859–861.

(5) Groves, J. T.; McClusky, G. A.; White, R. E.; Coon, M. J. Aliphatic Hydroxylation by Highly Purified Liver Microsomal Cytochrome P450. Evidence for Carbon Radical Intermediate. *Biochem. Biophys. Res. Commun.* **1978**, *81*, 154–160.

(6) Theorell, H. Crystalline Peroxidase. *Enzymologia* **1941**, *10*, 250–252.

(7) Keilin, D.; Mann, T. On the Haematin Compound of Peroxidase. *Proc. R. Soc. London, Ser. B* **1937**, *122B*, 119−133.

(8) Yosca, T. H.; Rittle, J.; Krest, C. M.; Onderko, E. L.; Silakov, A.; Calixto, J. C.; Behan, R. K.; Green, M. T. Iron(IV)hydroxide pK(a) and the Role of Thiolate Ligation in C-H bond Activation by Cytochrome P450. Science **2013**, *342*, 825−829.

(9) Huang, X.; Groves, J. T. Beyond Ferryl-Mediated Hydroxylation: 40 Years of the Rebound Mechanism and C-H Activation. *J. Biol. Inorg. Chem.*, **2017**, *22*, 185–207.

(10) Huang, X.; Groves, J. T. Oxygen Activation and Radical Transformations in Heme Proteins and Metalloporphyrins. *Chem. Rev.* **2018**, *118*, 2491–2553.

(11) Groves, J. T. Key Elements of the Chemistry of Cytochrome P-450: The Oxygen Rebound Mechanism. *J. Chem. Educ.* **1985**, *62*, 928–931.

(12) Tang, M.-C.; Zou, Y.; Watanabe, K.; Walsh, C. T.; Tang, Y. Oxidative Cyclization in Natural Product Biosynthesis. *Chem. Rev.* **2016**, *117*, 5226–5333.

(13) Walsh, C. T.; Tang, Y. Recent Advances in Enzymatic Complexity Generation: Cyclization Reactions. *Biochemistry*. **2018**, *57*, 3087–3104.

(14) Guengerich, F. P.; Munro, A. W. Unusual Cytochrome P450 Enzymes and Reactions. *J. Biol. Chem.* **2013**, *288*, 17065–17073.

(15) Walsh, C. T.; Moore, B. S. Enzymatic Cascade Reactions in Biosynthesis. *Angew. Chem. Int. Ed.* **2019**, *58*, 6846–6879.

(16) McCormick, M. H.; Stark, W. M.; Pittenger, G. E.; Pittenger, R. C.; McGuire, J. M. Vancomycin, A New Antibiotic. I. Chemical and Biologic Properties. *Antibiot. Annu.* **1955-1956, *3*,** 606–611**.**

(17) Levine, D.P. Vancomycin: A History. *Clin. Infect. Dis.* **2006**, *42*, S5–S12.

(18) Butler, M.S; Hansford, K. A.; Blaskovich, M. A. T.; Halai, R.; Cooper, M. A. *J. Antibiot.* Glycopeptide Antibiotics: Back to the Future. **2014**, *67*, 631–644.

(19) Williams, D. H.; Bardsley, B. The Vancomycin Group of Antibiotics and the Fight against Resistant Bacteria. *Angew. Chem. Int. Ed.* **1999**, *38*, 1172–1193.

(20) Zerbe, K.; Woithe, K.; Li, D. B.; Vitali, F.; Bigler, L.; Robinson, J. A. An Oxidative Phenol Coupling Reaction Catalyzed by OxyB, a Cytochrome P450 from the Vancomycin-Producing Microorganism. *Angew. Chem. Int. Ed.* **2004**, *43*, 6709–6713.

(21) Woithe, K.; Geib, N.; Zerbe, K.; Li, D.B.; Heck, M.; Fournier-Rousset, S.; Meyer, O.; Vitali, F. Matoba, N. Abou-Hadeed, K. Robinson, J. A. Oxidative Phenol Coupling Reactions Catalyzed by OxyB: A Cytochrome P450 from the Vancomycin Producing Organism. Implications for Vancomycin Biosynthesis. *J. Am. Chem. Soc.* **2007**, *129*, 6887–6895.

(22) Forneris, C. C.; Ozturk, S.; Gibson, M. I.; Sorensen, E. J.; Seyedsayamdost, M. R. *In Vitro* Reconstitution of OxyA Enzymatic Activity Clarifies Late Steps in Vancomycin Biosynthesis. *ACS Chem. Biol.* **2017**, *12*, 2248–2253.

(23) Forneris, C. C.; Seyedsayamdost, M. R. In Vitro Reconstitution of OxyC Activity Enables Total Chemoenzymatic Syntheses of Vancomycin Aglycone Variants. *Angew. Chem. Int. Ed.* **2018**, *57*, 8048–8052.

(24) Yim, G.; Thaker, M. N.; Koteva, K.; Wright, G. Glycopeptide Antibiotic Biosynthesis. *J. Antibiot.* **2014,** *67,* 31–41.

(25) Stegmann, E.; Frasch, H.-J.; Wohlleben, W. Glycopeptide Biosynthesis in the Context of Basic Cellular Functions. *Curr. Opin. Microbiol.* **2010**, *13*, 595–602.

(26) Hohenberger, J.; Meyer, K. The Biology and Chemistry of High-Valent Iron-Oxo and Iron-Nitrido Complexes. *Nat. Commun.* **2012**, *3*, 720.

(27) Groves, J. T. High-Valent Iron in Chemical and Biological Oxidations. *J. Inorg. Biochem.* **2006**, *100*, 434–447.

(28) Nam, W. High-Valent Iron(IV)-Oxo Complexes of Heme and Non-Heme Ligands in Oxygenation Reactions. *Acc. Chem. Res.* **2007**, *40*, 522–531.

(29) Bollinger, J. M., Jr.; Krebs, C. Stalking Intermediates in Oxygen Activation by Iron Enzymes: Motivation and Method. *J. Inorg. Biochem.* **2006**, *100*, 586–605.

(30) Greule, A.; Izoré, T.; Machell, D.; Hansen, M. H.; Schoppet, M.; De Voss, J. J.; Charkoudian, L. K.; Schittenhelm, R. B.; Harmer, J. R.; Cryle, M. J. The Cytochrome P450 OxyA from the Kistamicin Biosynthesis Cyclization Cascade is Highly Sensitive to Oxidative Damage. *Front. Chem.* **2022**, *10*, 868240.

(31) Nordblom, G. D.; White, R. E.; Coon, M. J. Studies on Hydroperoxide-Dependent Substrate Hydroxylation by Purified Liver Microsomal Cytochrome P450. *Arch. Biochem. Biophys.* **1976**, *175*, 524–533.

(32) Joo, H.; Lin, Z.; Arnold, F. H. Laboratory Evolution of Peroxide-Mediated Cytochrome P450 Hydroxylation. *Nature*. **1999**, *399*, 670–673.

(33) Grant, J. L.; Hsieh, C. H.; Makris, T. M. Decarboxylation of Fatty Acids to Terminal Alkenes by Cytochrome P450 Compound I. *J. Am. Chem. Soc.* **2015**, *137*, 4940–4943.

(34) Davydov, R.; Kappl, R.; Hüttermann, J.; Peterson, J. A. EPR Spectroscopy of Reduced Oxyferrous P450$_{cam}$. *FEBS Lett.* **1991**, *295*, 113–115.

(35) Davydov, R.; Makris, T. M.; Kofman, V.; Werst, D. E.; Sligar, S. G.; Hoffmann, B. M. Hydroxylation of Camphor by Reduced Oxy-Cytochrome P450$_{cam}$: Mechanistic Implications of EPR and ENDOR Studies of Catalytic Intermediates in Native and Mutant Enzymes. *J. Am. Chem. Soc.* **2001**, *123*, 1403–1415.

(36) Denisov, I. G.; Makris, T. M.; Sligar, S. G. Cryotrapped Reaction Intermediates of Cytochrome P450 Studied by Radiolytic Reduction with Phosphorous-32. *J. Biol. Chem.* **2001**, *276*, 11648–11652.

(37) Rittle, J.; Green, M. T. Cytochrome P450 Compound I: Capture, Characterization, and C-H Bond Activation Kinetics. *Science*. **2010**, *330*, 933–937.

(38) Isin, E. M.; Guengerich, F. P. Substrate Binding to Cytochrome P450. *Anal. Bioanal. Chem.* **2008**, *392*, 1019–1030.

(39) Haslinger, K.; Peschke, M.; Brieke, C.; Maximowitsch, E.; Cryle, M. J. X-Domain of Peptide Synthetases Recruits Oxygenases Crucial for Glycopeptide Biosynthesis. **2015**, *Nature*, *521*, 105–109.

(40) Krest, C. M.; Onderko, E. K.; Yosca, T. H.; Calixto, J. C.; Karp, R. F.; Livada, J.; Rittle, J.; Green, M. T. Reactive Intermediates in Cytochrome P450 Catalysis. *J. Biol. Chem.*, **2013**, *288*, 17074–17081.

(41) Wang, X.; Peter, S.; Kinne, M.; Hofrichter, M.; Groves, J. T. Detection and Kinetic Characterization of a Highly Reactive Heme-Thiolate Peroxygenase Compound I. *J. Am. Chem. Soc.* **2012**, *134*, 12897−12900.

(42) Palcic, M. M.; Rutter, R.; Araiso, T.; Hager, L. P.; Dunford, H. B. The Spectrum of Chloroperoxidase Compound I. *Biochem. Biophys. Res. Commun.* **1980**, *94*, 1123–1127.

(43) Egawa, T.; Proshlyakov, D. A.; Miki, H.; Makino, R.; Ogura, T.; Kitagawa, T.; Ishimura, Y. Effects of a Thiolate Axial Ligand on the π → π* Electronic States of Oxoferryl Porphyrins: A Study of the Optical and Resonance Raman Spectra of Compounds I and II of Chloroperoxidase. *J. Biol. Inorg. Chem*. **2001**, *6*, 46–54.

(44) Dornevil, K.; Davis, I.; Fielding, A. J.; Terrell, J. R.; Ma, L. Liu, A. Cross-linking of Dicyclotyrosine by the Cytochrome P450 Enzyme CYP121 from *Mycobacterium tuberculosis* proceeds through a Catalytic Shunt Pathway. *J. Biol. Chem.* **2017**, *292*, 13645–13657.

(45) Rittle, J.; Younker, J. M.; Green, M. T. Cytochrome P450: The Active Oxidant and Its Spectrum. *Inorg. Chem.* **2010**, *49*, 3610–3617.

(46) Tsai, R.; Yu, C. A.; Gunsalus, I. C.; Peisach, J.; Blumberg, W.; Orme-Johnson, W. H.; Beinert H. Spin-State Changes in Cytochrome

$P450_{cam}$ on Binding of Specific Substrates. *Proc. Natl. Acad. Sci. U. S. A.* **1970**, *66*, 1157–1163.

(47) Lipscomb, J. D. Electronic Paramagnetic Resonance Detectable States of Cytochrome $P\text{-}450_{cam}$. **1980**, *19*, 3590–3599.

(48) Fielding, A. J.; Dornevil, K.; Ma, L.; Davis, I.; Liu. A. Probing Ligand Exchange in the P450 Enzyme CYP121 from *Mycobacterium tuberculosis*: Dynamic Equilibrium of the Distal Heme Ligand as a Function of pH and Temperature. *J. Am. Chem Soc.* **2017**, *139*, 17484 –17499.

(49) It is well-documented that there is a temperature-dependent thermodynamic equilibrium between the high- and low-spin ferric heme states (see ref. 48). Cryogenic freezing of EPR samples in liquid nitrogen favors the formation of the substrate-bound, low-spin ferric heme state consistent with type II-like binding.

(50) Rutter, R.; Hager, L. P.; Dhonau, H.; Hendrich, M.; Valentine, M.; Debrunner, P. Chloroperoxidase Compound I: Electronic Paramagnetic Resonance and Mössbauer Studies. *Biochemistry*. **1984**, *23*, 6809 –6816.

(51) Schulz, C. E.; Devaney, P. W.; Winkler, H.; Debrunner, P. G.; Doan, N.; Chiang, R.; Rutter, R.; Hager, L. P. Horseradish Peroxidase Compound I: Evidence for Spin Coupling between the Heme Iron and a 'Free' Radical. **1979**, *103*, 102–105.

(52) Goldfarb, D.; Stoll, S. *EPR Spectroscopy: Fundamentals and Methods*; Eds.; Wiley: 2018.

(53) Orbach, R. Spin-Lattice Relaxation in Rare-Earth Salts. *Proc. R. Soc. Ser. A.* **1961**, *264*, 458–484.

(54) Orbach, R. Spin-Lattice Relaxation in Rare-Earth Salts: Field Dependence of the Two Phonon Process. **1961**, *Proc. R. Soc. Ser. A. 264*, 485–495.

(55) Ballou, D. P.; Palmer, G. A. Practical Rapid Quenching Instrument for the Study of Reaction Mechanisms by Electron Paramagnetic Resonance Spectroscopy. *Anal. Chem.* **1974**, *46*, 1248–1253.

(56) Krest, C. M.; Silakov, A. S.; Rittle, J.; Yosca, T. H.; Onderko, E. L.; Calixto, J. C.; Green, M. T. Significantly Shorter Fe-S Bond in Cytochrome P450-I is Consistent with Greater Reactivity Relative to Chloroperoxidase. *Nat. Chem.* **2015**, *7*, 696–702.

(57) Onderko, E. L.; Silakov, A.; Yosca, T. H.; Green, M. T. Characterization of a Selenocysteine-Ligated P450 Compound I Reveals Direct Link between Electron Donation and Reactivity. *Nat. Chem*. **2017**, *9*, 623–628.

(58) Given a typical ferryl zero-field splitting value D of 40 cm^{-1} (see ref. 56), and an experimentally derived $g_{\perp}^{eff}$ of 1.995, an exchange-coupling constant J of approximately 56 cm^{-1} is obtained for the OxyB cpd-I system. The derived J/D for OxyB is only slightly larger (~10%) than that of CYP119 and significantly greater than that of CPO (~40%).

(59) Winkler, J. R.; Gray, H. B. Could Tyrosine and Tryptophan Serve Multiple Roles in Biological Redox Processes? *Phil. Trans. R. Soc. A.* **2015**, *373*, 1–7.

(60) Gray, H. B.; Winkler, J. R. Hole Hopping through Tyrosine/Tryptophan Chains Protects Proteins from Oxidative Damage. *Proc. Natl. Acad. Sci.* **2015**, *112*, 10920–10925.

(61) Gray, H. B.; Winkler, J. R. Functional and Protective Hole Hopping in Metalloenzymes. *Chem. Sci.* **2021**, *12*, 13988–14003.

(62) Forneris, C. C.; Nguy, A. K. L.; Seyedsayamdost, M. R. Mapping and Exploiting the Promiscuity of OxyB toward the Biocatalytic Production of Vancomycin Aglycone Variants. *ACS Catal.* **2020**, *10*, 9287–9298.

(63) Groves, J. T. Enzymatic C-H bond Activation: Using Push to Get Pull. *Nat. Chem.* **2014**, *6*, 89−91.

(64) Green, M. T.; Dawson, J. H.; Gray, H. B. Oxoiron(IV) in chloroperoxidase compound II is basic: Implications for P450 chemistry. *Science* **2004**, *304*, 1653−1656.

(65) Warren, J. J.; Tronic, T. A.; Mayer, J. M. Thermochemistry of Proton-Coupled Electron Transfer Reagents and its Implications. *Chem. Rev.* **2010**, *110*, 6961−7001.

(66) Reece, S. Y.; Hodgkiss, J. M.; Stubbe, J.; Nocera, D. G. Proton-Coupled Electron Transfer: The Mechanistic Underpinning for Radical Transport and Catalysis in Biology. *Phil. Trans. R. Soc. B.* **2006**, *361*, 1351–1364.

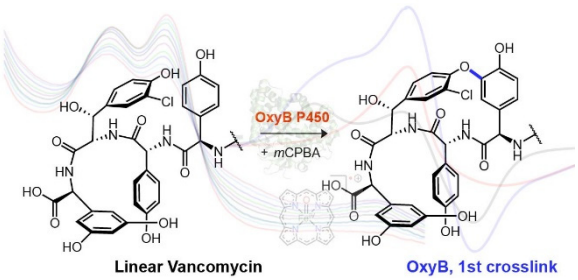

Supporting Information for

Detection of a Kinetically Competent Compound-I Intermediate in the Vancomycin Biosynthetic Enzyme OxyB

Andy K. L. Nguy[†], Ryan J. Martinie[†,¶], Amanda Cai[†], and Mohammad R. Seyedsayamdost[†,‡,*]

[†]Department of Chemistry, Princeton University, Princeton, NJ 08544, United States
[‡]Department of Molecular Biology, Princeton University, Princeton, NJ 08544, United States
*Correspondence: mrseyed@princeton.edu

Materials

Ampicillin, IPTG, PMSF, lysozyme, protease inhibitor cocktail, Sephadex G-25, COMU, NEt_3, DIPEA (Hünig's base), TIS, DBU, TFA, formic acid (FA), Fmoc-OSu, hydrazine monohydrate, $NaNO_2$, DMF, DCM, Sodium dithionite, HCl, guanidine hydrochloride, *meta*-Chloroperoxybenzoic acid (*m*CPBA) were purchased from Millipore-Sigma. Commercially available Fmoc- and side chain-protected amino acids, 2-chlorotriyl chloride resin, and other reagents for solid-phase peptide synthesis were purchased from Novabiochem/EMD Millipore and Sigma-Aldrich. LB broth, Terrific Broth, LB agar, δ-aminolevulinic acid hydrochloride, rhamnose monohydrate, DNAse I, tris base, imidazole, glycerol, potassium phosphate monobasic, potassium phosphate dibasic, sodium hydroxide, and HisPur™ Ni-NTA resin were purchased from Fisher Scientific. Liquid isopentane was purchased from multiple vendors, including VWR, Neta, Sigma-Aldrich and Fisher. Coenzyme A was purchased from CoALA Biosciences. 4 mm Thin Wall Quartz EPR Sample Tubes(250 mm long) were purchased from Wilmad-LabGlass. The Stopped-Flow Module (SFM) 3000, the freeze-quench accessory and the EPR collection kit (which includes ejection nozzle, EPR funnel, ageing loops and packing rods) were purchased from BioLogic. Liquid He was supplied by Princeton Physics Department and Airgas.

General Procedures

All UV–vis spectra were acquired on a Cary 60 UV–visible spectrophotometer (Agilent). Low resolution high-performance liquid chromatography-mass spectrometry (HPLC-MS) analysis was performed on an Agilent instrument consisting of a liquid autosampler, a 1260 Infinity Series HPLC system coupled to a diode array detector, and a 6120 Series Single Quadrupole ESI mass spectrometer. High-resolution (HR) HPLC-MS was carried out on an Agilent UHD Accurate Mass quadrupole time-of-flight (Q-TOF) LC-MS system, equipped with a 1260 Infinity Series HPLC, an automated liquid sampler, a photodiode array detector, a JetStream ESI source and a 6540 Series UHD Accurate-Mass Q-TOF mass spectrometer. HPLC purifications were carried out on an Agilent 1260 Infinity Series analytical HPLC system equipped with a temperature-controlled column compartment, a diode array detector, an automated fraction collector, and an automated liquid sampler.

Electron paramagnetic resonance (EPR) spectra were acquired at the Princeton University Department of Chemistry facilities. CW X-band EPR spectra were recorded at 10 K on a Bruker EMXplus EPR spectrometer equipped with an Oxford Liquid Helium cryostat. In general, the following parameters were used: power, 50 μW to 10 mW; modulation amplitude, 5 G; modulation frequency, 100 kHz; center field, 3200 G; sweep width, 1500 G; sweep time, 60 s; 10 scans. All EPR spectra were simulated using the "pepper" utility from the EasySpin software package with the Kazan Viewer user-interface from PennState.

Expression of OxyB

OxyB was expressed according to previously described procedures.[1,2] Briefly, a 14-mL sterile culture tube containing 5 mL LB supplemented with Amp (100 μg/mL) was inoculated with a single colony of *E. coli* KRX harboring *oxyB*-pET-15b. The 5 mL cultures were grown at 37°C and 200 RPM for at least 12 hours, at which point 500 μL (1% v/v) were used to inoculate 50 mL LB-Amp in a 250 mL Erlenmeyer flask. The intermediate culture was grown overnight at 37°C and 200 RPM, and subsequently used to inoculate large cultures. Erlenmeyer flasks (8 x 4L) containing

800 mL of TB supplemented with ampicillin were inoculated with 4 mL (0.5% v/v) of intermediate culture. The large-scale cultures were grown at 37°C/200 RPM to an $OD_{600\ nm}$ ~0.6, cooled in an ice bath for 5–10 minutes and supplemented with δ-aminolevulinic acid to a final concentration of 0.5 mM. The cultures were grown for an additional 20 min at 18°C/200 RPM, and then supplemented with a final concentration of 0.2 mM of IPTG and 0.1% (v/v) rhamnose. After 24 h, the cells were harvested by centrifugation (8000g, 20 minutes, 4°C), frozen and stored at -80°C. A yield of 10 g of cell pellet per L culture was generally obtained.

Purification of OxyB

Purification steps were carried out at 4°C. Lysis buffer consisted of 50 mM Tris, 50 mM NaCl, 5 mM imidazole, 5% glycerol, pH 7.8. The cell pellet was resuspended in lysis buffer (5 mL/g) in 500 mL beaker. The suspension was supplemented with protease inhibitor cocktail (1 µL/mL), PMSF (0.25 mM), lysozyme (1 mg/mL) and DNase I (10 U/mL). Subsequently, the suspension was stirred for 30 min and sonicated on ice for 2 min in 15s on/15s off cycles at 30% power. The sonication cycle was repeated after the suspension rested on ice for 5 min. Typically, 4 to 5 total sonication cycles were performed. The cell debris was then pelleted by centrifugation (32,000g, 1 h, 4°C). PMSF (0.25 mM final concentration) was added to the clarified lysate, which was then loaded onto a nickel metal affinity column (15 mL), which had been equilibrated with lysis buffer. The column was washed with 10 CV of lysis buffer and 10 CV of medium wash buffer (50 mM Tris, 50 mM NaCl, 30 mM imidazole, 5% glycerol, pH 7.8). Finally, the protein was eluted with 10 CV of elution buffer (50 mM Tris, 50 mM NaCl, 300 mM imidazole, 5% glycerol, pH 7.8). His_6-OxyB was buffer exchanged on a Sephadex G-25 column (40 mL) that had been equilibrated with G25 buffer (50 mM KP_i, pH 7). The desired protein fractions, identified by the bright red color, were pooled and spin concentrated with an Amicon® Ultra-15 30 kDA MWCO spin concentrator until a final concentration of 25 mg/mL. 5 mL protein elution aliquots were subsequently loaded onto a BioRad NGC chromatography system equipped with a HiPrep 16/60 Sephacryl S-200 HR column, which was equilibrated in G25 buffer. His_6-OxyB was eluted via FPLC with G25 buffer at 0.3 mL/min flow rate. FPLC fractions that exhibited an elevated Reinheitszhal around 1.5 were pooled, spin concentrated, flash frozen in liquid N_2, and stored at -80°C. Final protein elution was analyzed by SDS-PAGE and UV/Vis spectroscopy for purity. The Reinheitszahl (Rz) purity ratio of A_{419}/A_{280} increased from ~1.2 to ~1.5 after FPLC-based purification. Based on an Rz of 1.5 and extinction coefficients of 100,000 $M^{-1}\,cm^{-1}$ (ferric heme) and 32,600 $M^{-1}\,cm^{-1}$ (OxyB), our purified consists of ~50% *holo*-OxyB. The final *holo*-OxyB concentration, rather than total OxyB, was used to calculate the amount of cpd-I formed in SF UV/Vis and RFQ-EPR experiments.

Synthesis and purification of 7mer peptide substrate

The synthesis of 7mer hydrazine substrates followed the method described previously.[2] Pure peptides were verified by HPLC-MS.

Synthesis and purification of Coenzyme A adducts of 7mer peptide

A 10 mM solution of 7mer peptide in a sparged 0.2 M sodium phosphate buffer containing 6 M guanidinium chloride at pH 3 was added to an Eppendorf tube equipped with a stir bar. The solution was cooled to -10°C in an ice/salt bath. Sodium nitrite (20 equiv.) was added to the reaction mixture, which was stirred for 30 min at -10°C. Coenzyme A (10 equiv.) was added to

the reaction mixture. Subsequently, the pH was adjusted to 6.8-7.0 with a micro-pH probe and the reaction was allowed to warm to room temperature and stir for 1 h.

The reaction was quenched with MeCN (+ 0.1% FA) to a final volume 1 mL. Purification of the peptide-CoA was achieved by repeated injection onto an analytical Phenomenex Luna C18 column (5 µm, 250 x 4.6 mm) that had been equilibrated with 10% MeCN in H_2O (+0.1% FA). The peptide-CoA adducts were eluted with a gradient 10-55% MeCN in H_2O (+0.1% FA) over 17 min. The purified material was verified by HR-HPLC-MS, aliquoted, and lyophilized.

Stopped-Flow UV/Vis Spectroscopy

Stopped-flow UV/Vis experiments were performed on a SX20 Applied Photophysics stopped-flow spectrometer, equipped with a 150W Xenon Lamp house, 4.65 nm/mm bandpass monochromator, a photodiode array accessory, and a PolyScience temperature controller water bath. For a single mixing experiment, 40 µM FPLC-purified OxyB (corresponding to 20 µM ferric *holo*-OxyB) and 2 mM *m*CPBA were loaded in separate syringes, and then rapidly mixed at 4°C or 20°C to give final concentrations of 10 µM ferric *holo*-OxyB and 1 mM *m*CPBA. Photodiode array spectra were taken over 1 s with 1000 timepoints in triplicate (at minimum). The first three SF-UV/Vis spectra were discarded by practice to push out the contents in the observation cell from the previous shot.

For a sequential mixing experiment, 40 µM OxyB (corresponding to 20 µM ferric *holo*-OxyB) and 550 µM mCPBA were loaded in separate syringes, rapidly mixed at 4°C, aged for 1s to promote the formation of OxyB cpd-I, and then rapidly mixed against variable concentrations of the 7mer-CoA adduct ranging from 40 µM to 160 µM. Note that excess *m*CPBA was necessary to promote maximal formation of cpd-I. The total drive volume was 400 ± 20 µL, the premix volume was 220 ± 10 µL, and the flush volume was 180 ± 10 µL with a 1 s delay time. Photodiode array spectra were taken over 1 s with 1000 timepoints in triplicate (at minimum).

Rapid Freeze-Quench EPR

A solution of 400 µM FPLC-purified OxyB (corresponding to 200 µM *holo*-OxyB) was rapidly mixed with 1 mM *m*CPBA (which was diluted from a 1 M *m*CPBA stock in MeCN) via the SFM-3000 module, which was maintained at 4°C by a Peltier water bath. The final concentrations were 200 µM *holo*-OxyB and 0.5 mM *m*CPBA. Underneath the ejection nozzle of the rapid freeze-quench accessory, a dewar with chilled isopentane equipped with a funnel and EPR tube was maintained near -140°C to -150°C via liquid nitrogen circulation. The ejected solution was rapidly quenched in chilled liquid isopentane to form snow-like crystals, which were packed into EPR tubes with rods pre-chilled in liquid nitrogen. RFQ-EPR samples were then transferred into a liquid nitrogen dewar for storage. RFQ-EPR timepoints were performed at least in duplicate.

RFQ-EPR sequences were typically divided into two phases: (1) the washing phase which pushed out the contents of the previous shot; and (2) collection phase to eject the solution into chilled isopentane bath. Special care was taken to ensure that the total volume of the washing phase constitutes at least 3 times the volume of the delay line to avoid dilution or cross contamination. Total flow rate was kept between 0.5 mL/s to 5 mL/s to establish adequate turbulent mixing conditions. Age time was calculated by assuming that fly time was 1 ms and that freeze time was 4 ms, which was subsequently added to the overall age time of the solution in the ageing hose. Delay lines were swapped out appropriately to modulate the age time.

Figure S1. Pseudo-1st order binding of OxyB to the X-PCP-7mer. Binding was monitored by the decay 419 nm Soret band after rapidly mixing 1 μM *holo*-OxyB with variable concentrations (40, 80, 100, 160, and 200 μM, left to right) of the X-PCP-7mer at RT in a single-mix SF-UV/Vis experimental set-up. The data were best fit to a single exponential; the fit parameters are shown.

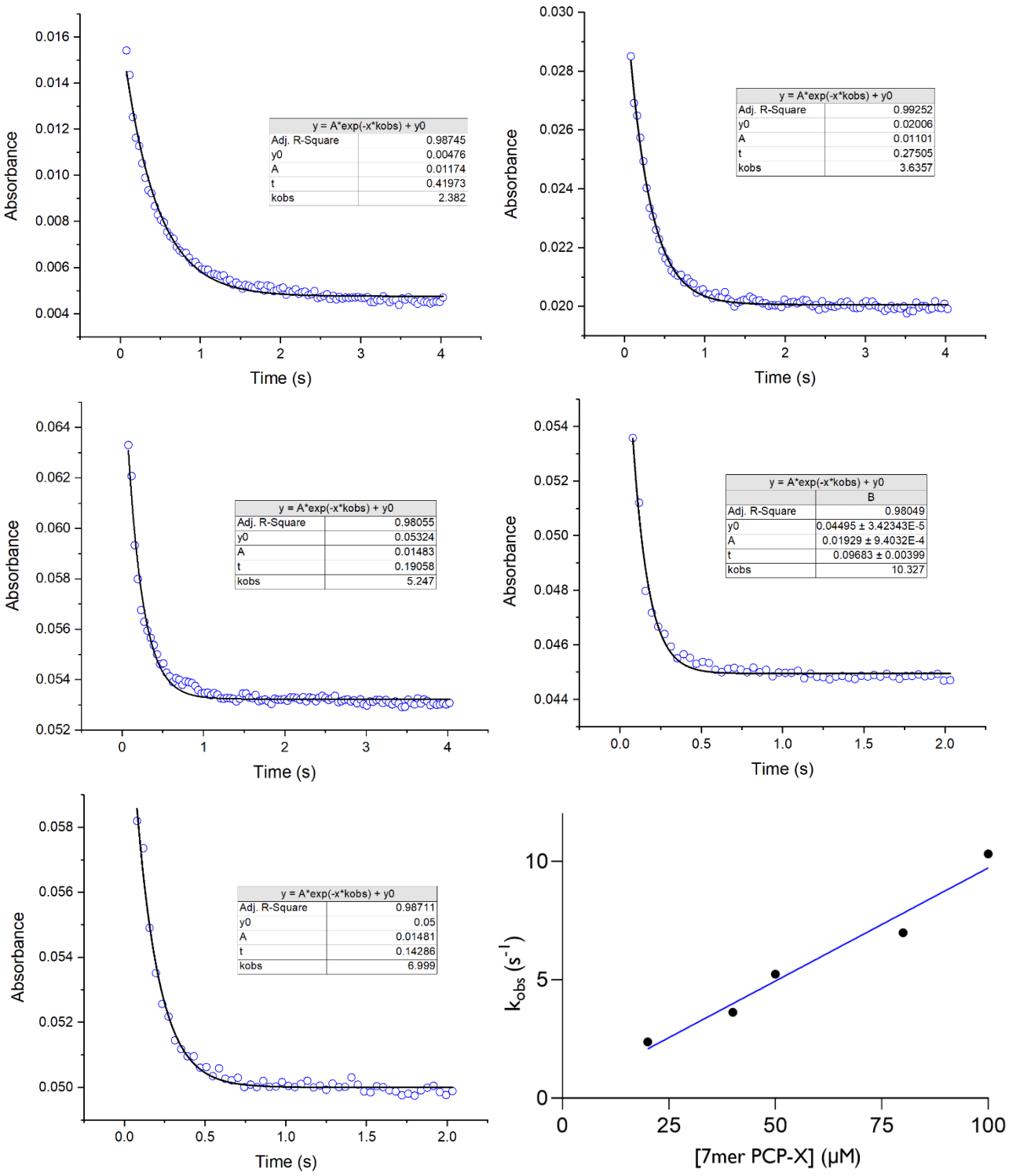

Figure S2. Difference UV/Vis spectra measured after reaction of the indicated concentration of X-PCP-7mer with OxyB.

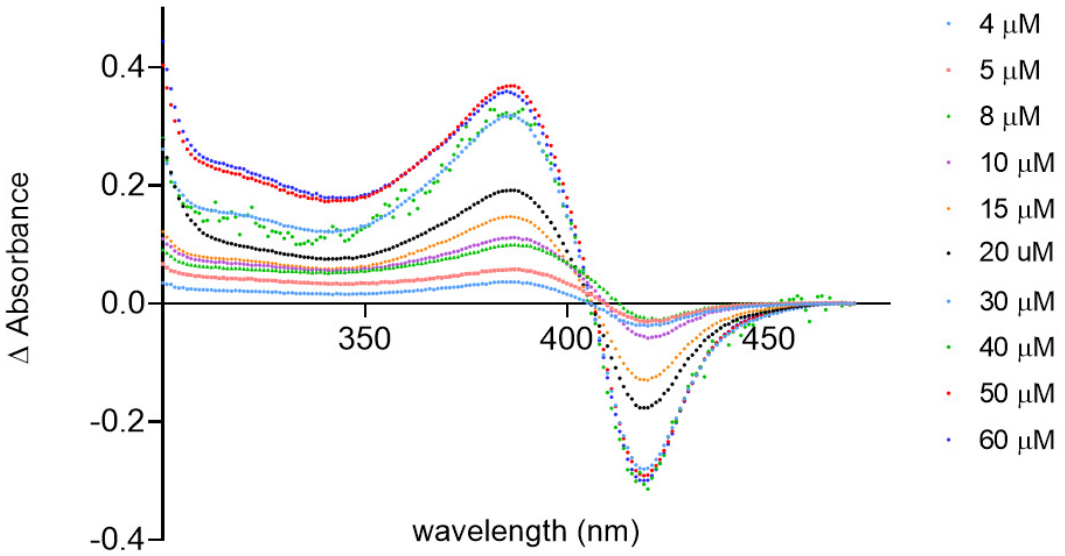

Figure S3. Reaction of as-isolated OxyB (40 μM total) with *m*CPBA (10 mM) monitored by stopped flow UV/Vis spectroscopy. Spectra at 1 ms and 500 ms are shown. No transient changes were observed.

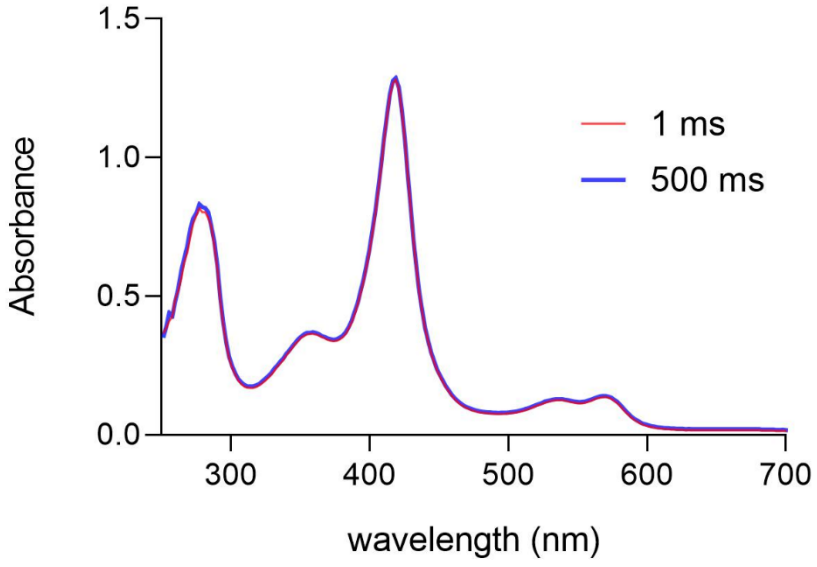

Figure S4. Further purification of as-isolated OxyB by size-exclusion FPLC chromatography. Prior to size-exclusion FPLC, as-isolated OxyB has a Reinheitszahl of ~1.2. The right peak (at 660 mL) contains OxyB with a superior Reinheitszahl value of ~1.5. The left peak at ~635 mL is predominantly *apo*-OxyB.

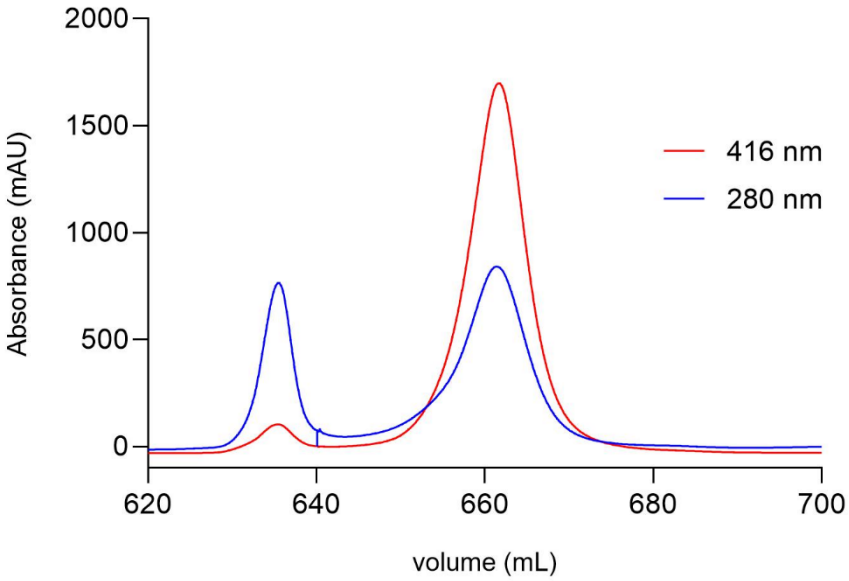

Figure S5. Derivation of the projection operator for target testing. A projection operator (P) can be used to determine whether a species is involved in the reaction via target testing. For $P = U' \cdot U'^{T}$, U' is the first k column vector in the U matrix obtained from SVD. Let $Y = P \cdot X$ where X is the target vector for a species. If target testing returns the original vector (i.e. Y = X), then (1) the species X is an active species in the reaction or (2) the input vector is a linear combination of the spectra of species involved in the reaction. The latter is highly improbable. The proof for the projection matrix can be found below.

Derivation of projection operator

Let S be the subspace of $\mathbb{R}^n$ with basis $\{\vec{s_1}, \vec{s_2}, \ldots, \vec{s_k}\}$.

Define:

$$\underset{nxk}{D} = \begin{bmatrix} | & | & & | \\ s_1 & s_2 & \ldots & s_k \\ | & | & & | \end{bmatrix}$$

Note that any $\vec{d} \in S$ can be represented $D\vec{y} = \vec{d}$ for some $\vec{y} \in \mathbb{R}^k$. Because $proj_S\vec{x} \in S$ for any $\vec{x} \in \mathbb{R}^n$, $proj_S\vec{x} = D\vec{y}$.

$$\vec{x} = proj_S\vec{x} + proj_{S^\perp}\vec{x}$$

$$\vec{x} - proj_S\vec{x} = proj_{S^\perp}\vec{x} \in S^\perp$$

The column space of D is the subspace S. Thus, the orthogonal complement of the column space of D is the subspace $S^\perp$. Therefore, the null space of $D^T = S^\perp$.

$$\vec{x} - proj_S\vec{x} \in N(D^T)$$

$$D^T(\vec{x} - proj_S\vec{x}) = \vec{0}$$

$$D^T\vec{x} - D^T proj_S\vec{x} = \vec{0}$$

Recall, $proj_S\vec{x} = D\vec{y}$ for $\vec{y} \in \mathbb{R}^k$

$$D^T\vec{x} - D^T D\vec{y} = \vec{0}$$

$$\vec{y} = (D^T D)^{-1} D^T\vec{x}$$

Therefore:

$$\boxed{proj_S\vec{x} = D(D^T D)^{-1} D^T\vec{x}}$$

Note that $D^T D$ will always be invertible because the columns of D are linearly independent.

We can now use singular value decomposition (SVD) to find the projection of $\vec{x}$ onto subspace S. Following SVD, $D = U\Sigma V^T$. By nature of SVD, U and V are both orthonormal bases, thus $U^T U = UU^T = I_n$ and $V^T V = VV^T = I_k$

$$D^T D = (U\Sigma V^T)^T(U\Sigma V^T) = V\Sigma^T U^T U\Sigma V^T = V\Sigma^2 V^T$$

$$(D^T D)^{-1} = V\Sigma^{-2} V^T$$

$$P = D(D^T D)^{-1} D^T = U\Sigma V^T V\Sigma^{-2} V^T V\Sigma^T U^T = U\Sigma\Sigma^{-2}\Sigma^T U^T = U \begin{bmatrix} I_k & 0 \\ 0 & 0 \end{bmatrix} U^T = \boxed{U'U'^T}$$

where P is a projection operator and U' is the first k column vectors in the U matrix.

Figure S6. Target testing confirmed that ferric OxyB and cpd-I are present in the original OxyB *m*CPBA shunt SF-UV/Vis spectra (see Fig. 2C). As shown, the ferric OxyB target vector (left panel) is returned with a near-identical projection vector. Similarly, the CYP119 cpd-I target vector (right panel) is returned with a matching projection vector.

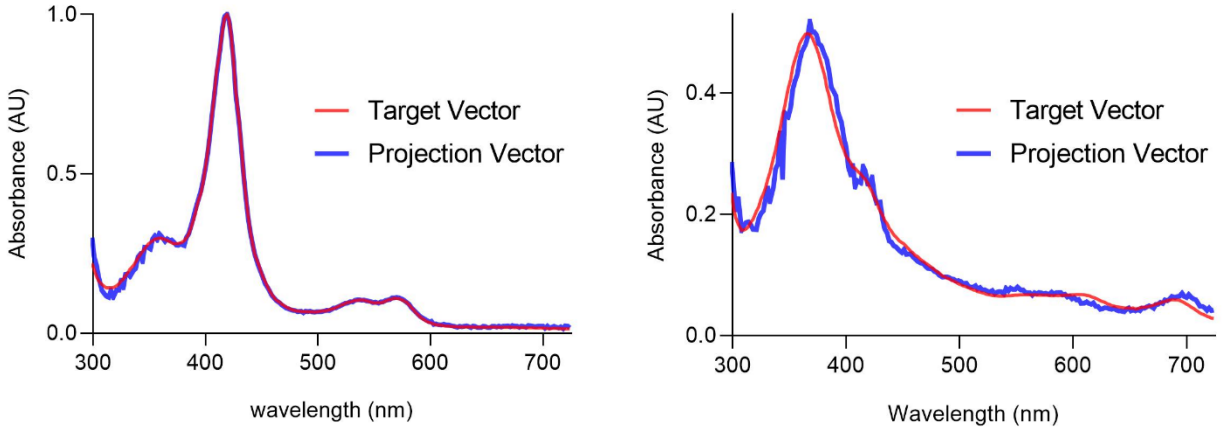

Figure S7. Singular value decomposition analysis of the reaction of OxyB with *m*CPBA. The singular values from the SF UV/Vis data matrix are the following: [9.81190296, 0.87190688, 0.09147521, 0.05005056, 0.01984731, 0.00765395, 0.00408359, 0.00400342, 0.00308753, 0.0028924]. Two significant singular values imply two predominant chemical species are present in the SF-UV/Vis spectra. As shown below, the abstract spectra associated with the first and second singular values are displayed (left panel). This is in good agreement with reported abstract spectra for CPO and CYP119 shunts.[3] Furthermore, linear combinations of abstract spectra from the OxyB *m*CPBA shunt data matrix recapitulate the CYP119 cpd-I target vector (right panel).

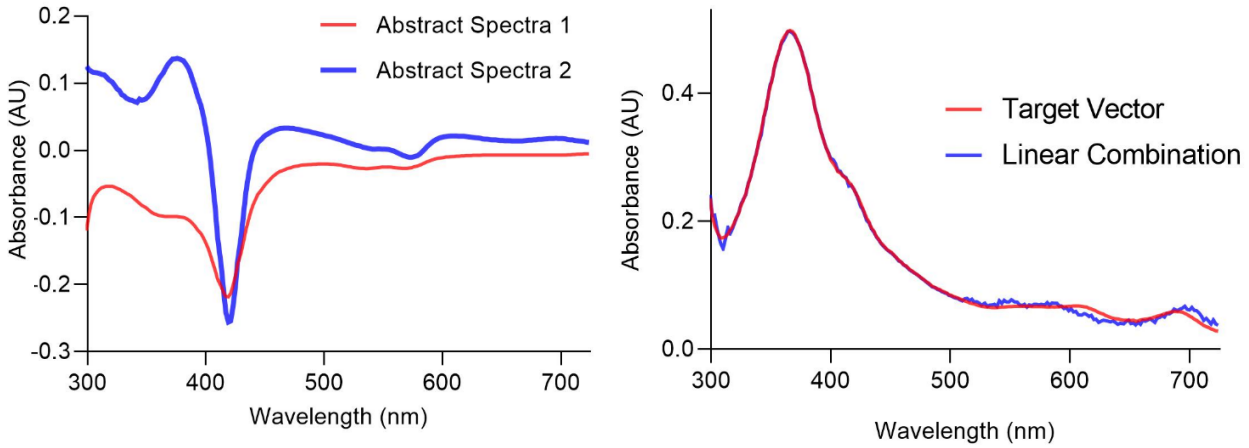

Figure S8. Stopped-Flow UV/Vis assessment of final concentrations of 10 μM *holo*-OxyB with 1 mM excess *m*CPBA at 4°C. Shown are full photodiode array UV/Vis spectra as a function time (top) and the UV/Vis difference absorption spectrum obtained from subtracting the diode array spectrum at 1 ms from that at 400 ms (middle). A feature diagnostic for cpd-I with a λ_{max} at 695 nm is obtained, similar to the results from experiments conducted at 20°C (see Fig. 2F). As in Fig. S6, target testing confirms the presence of cpd-I in this dataset (bottom). The kinetics at 4°C are also biphasic with fast (80.4 s^{-1}, 0.15 AU at 419 nm) and slow (4.7 s^{-1}, 0.49 AU at 419 nm) phases. The amplitude change suggests that 64% of available ferric heme generated cpd-I, thus a ~1.5-fold greater yield relative to 20°C.

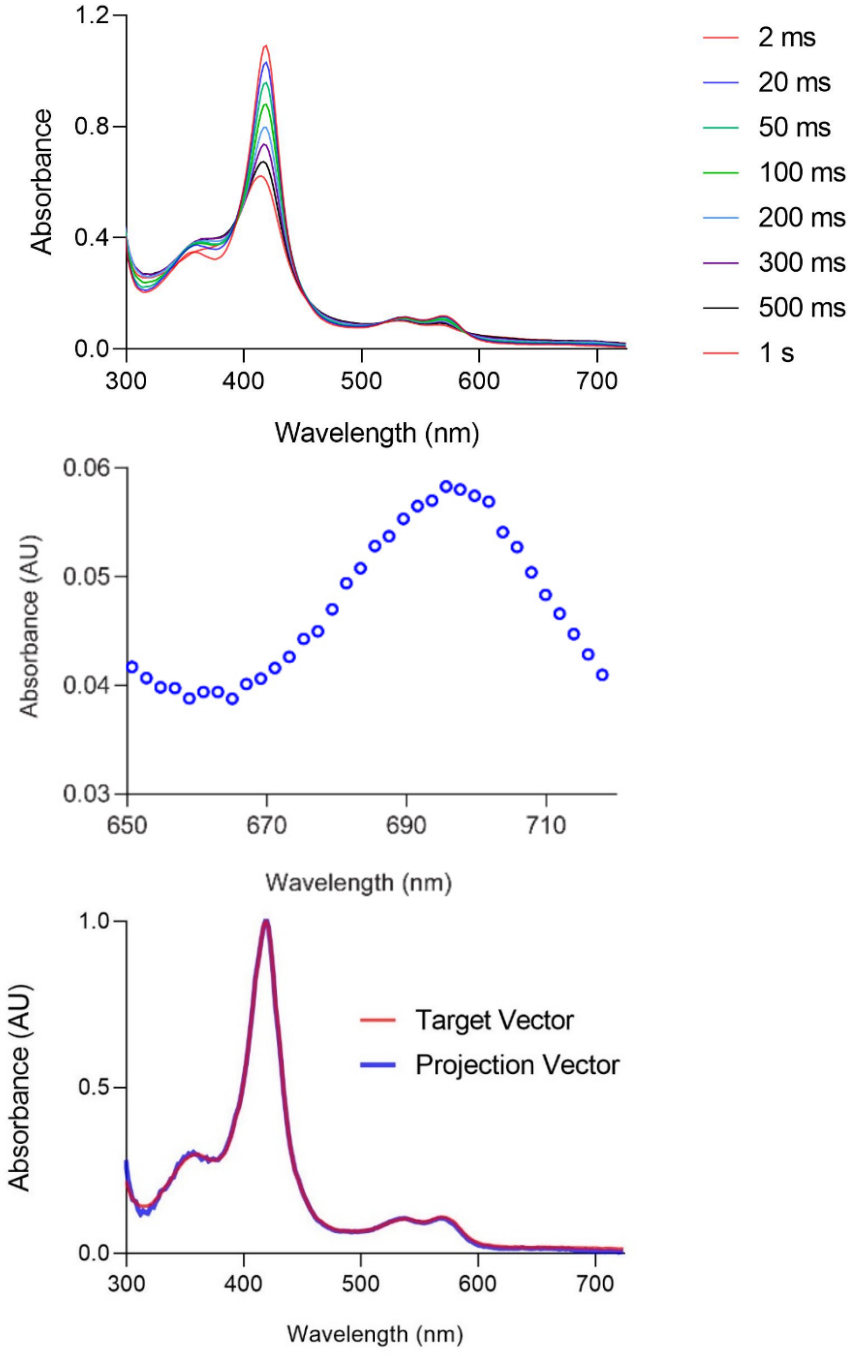

Figure S9. CW X-band EPR spectrum of *holo*-OxyB (100 μM) in the presence of X-PCP-7mer (300 μM). Simulations to the high-spin (top) and low-spin (bottom) components are shown in red. See main text for simulation parameters.

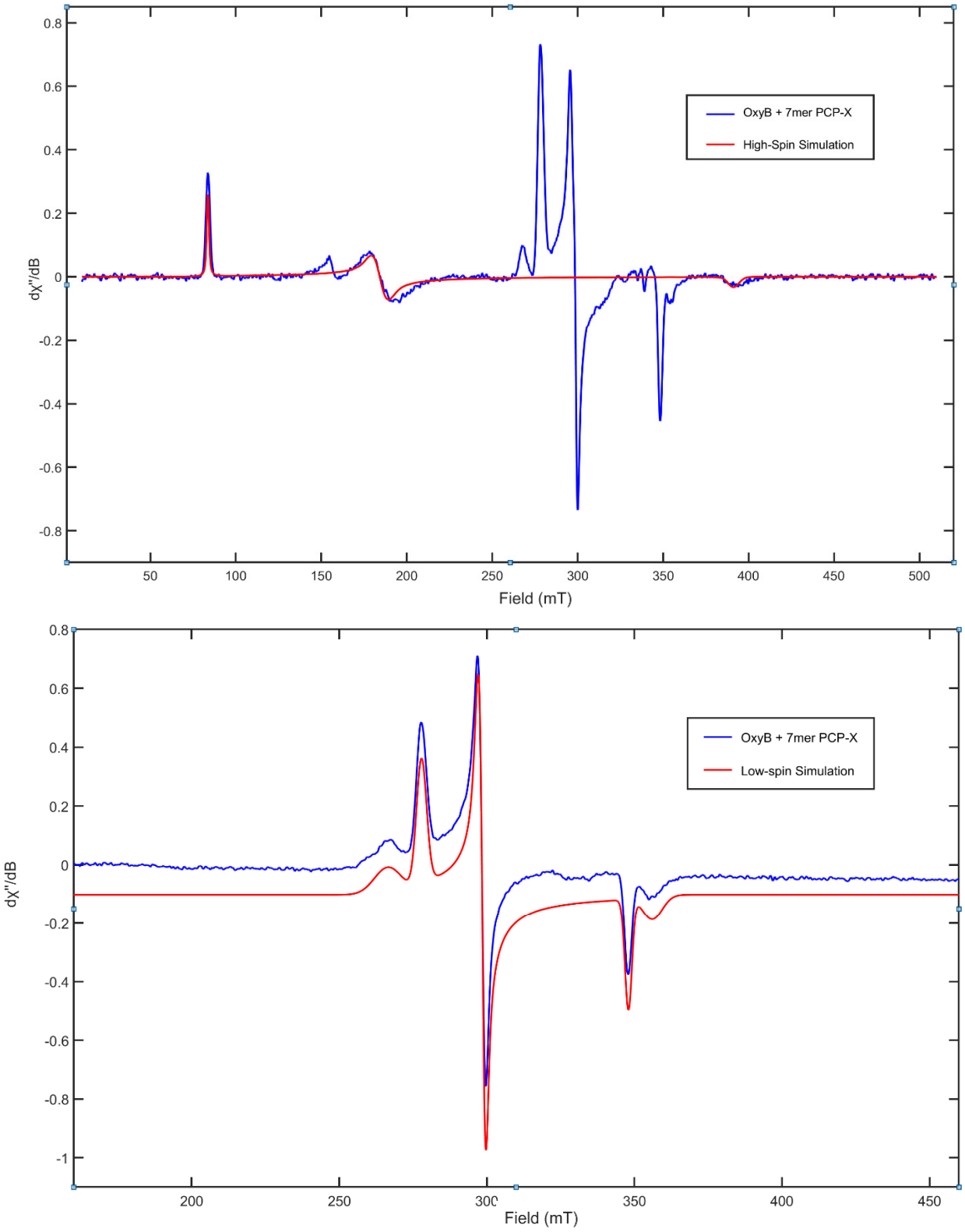

Figure S10. CW X-band EPR spectrum of *holo*-OxyB (100 μM) with increasing concentrations of the X-PCP-7mer. The intensity of both substrate-dependent high- and low-spin features (see Fig. S5) are enhanced with increasing substrate concentrations.

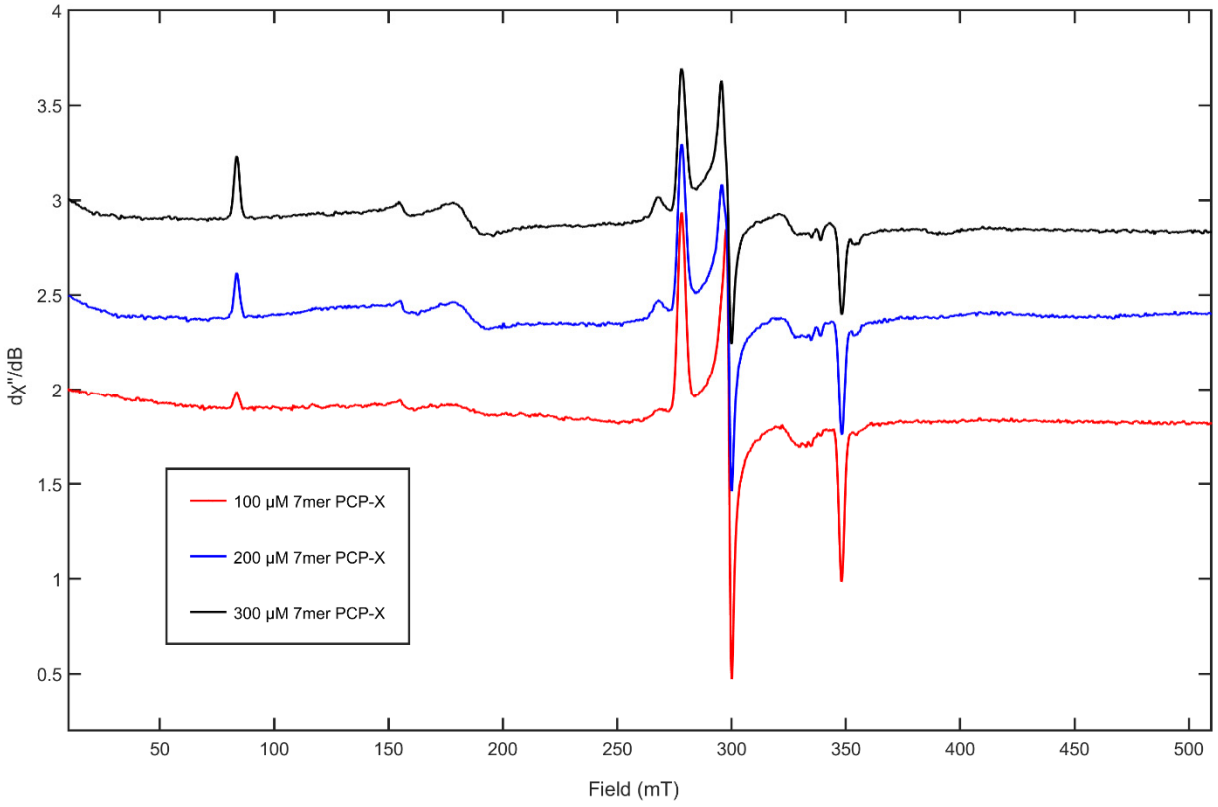

Figure S11. EPR power dependence of the cpd-I composite spectrum after mixing *holo*-OxyB with *m*CPBA to give final concentrations of 100 μM and 0.5 mM, respectively, and quenching at 70 ms. EPR spectra were collected at 10 K.

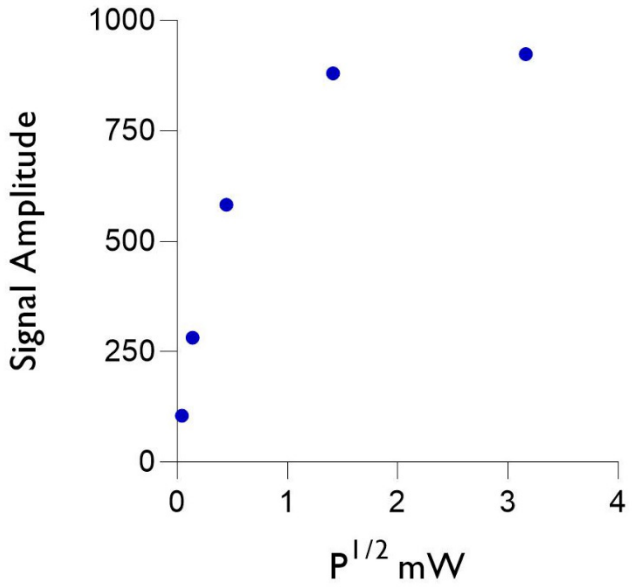

Figure S12. Power saturation profiles of the composite spectrum of cpd-I and paramagnetic contaminant at 7 K. The samples were generated as described in Methods by quenching a reaction with final concentrations of 100 μM *holo*-OxyB and 0.5 mM mCBPA at 70 ms. EPR spectra were then recorded at 7 K as a function of power as indicated. The profiles are shown in three regimes, low (top, 2 μW–10 mW), medium (middle, 10–80 mW), and high power (bottom, 100–200 mW).

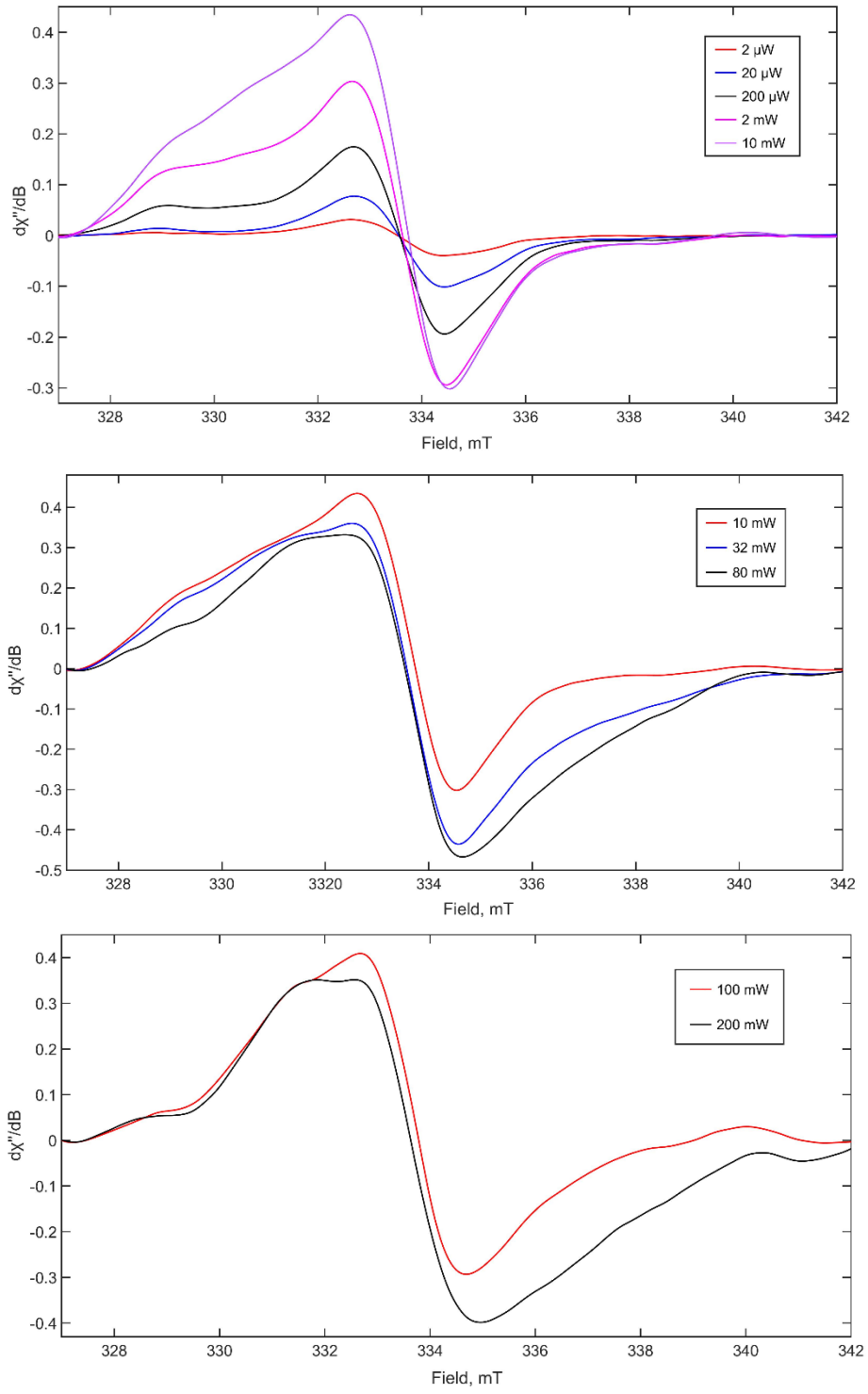

Figure S13. Simulation of cpd-I spectra after RFQ-EPR spectroscopic assessment of OxyB (100 μM final *holo*-OxyB) with *m*CPBA (0.5 mM final) and quenching at the times indicated. Similar spectra are observed at each timepoint. As in the SF UV/Vis experiment (Fig. 2E), optimal cpd-I signal is observed at the 70 ms timepoint.

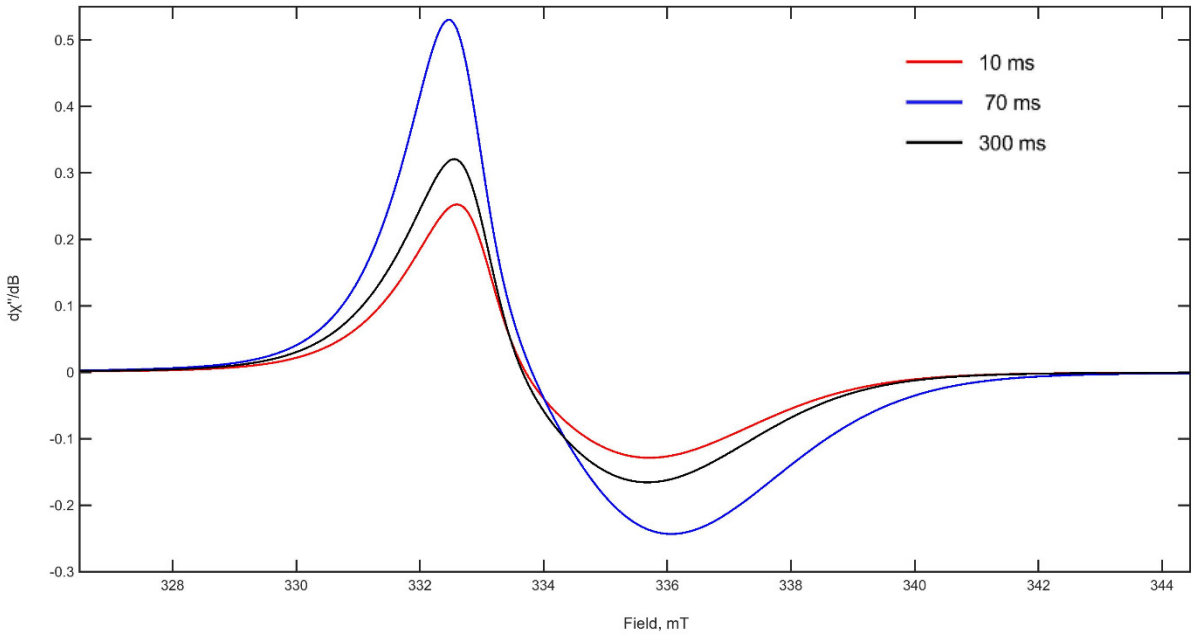

Figure S14. Sequential mix SF-UV/Vis spectroscopy to monitor reaction of the cpd-I in OxyB with 7mer-CoA: 20 μM *holo*-OxyB was rapidly mixed with 0.5 mM mCPBA, aged for 1 s, and subsequently pushed against variable concentrations of 7mer-CoA (ranging from 40 μM to 160 μM. The reaction was monitored at the Soret band (419 nm) and the traces were best fit to single exponential kinetics. Excess *m*CPBA was necessary to promote maximal formation of cpd-I. The auto-decay rate constant is ~0.4 s^{-1}. The parameters are shown for each concentration. Amplitudes, A; time constants, τ; observed rate constants, k_{obs}.

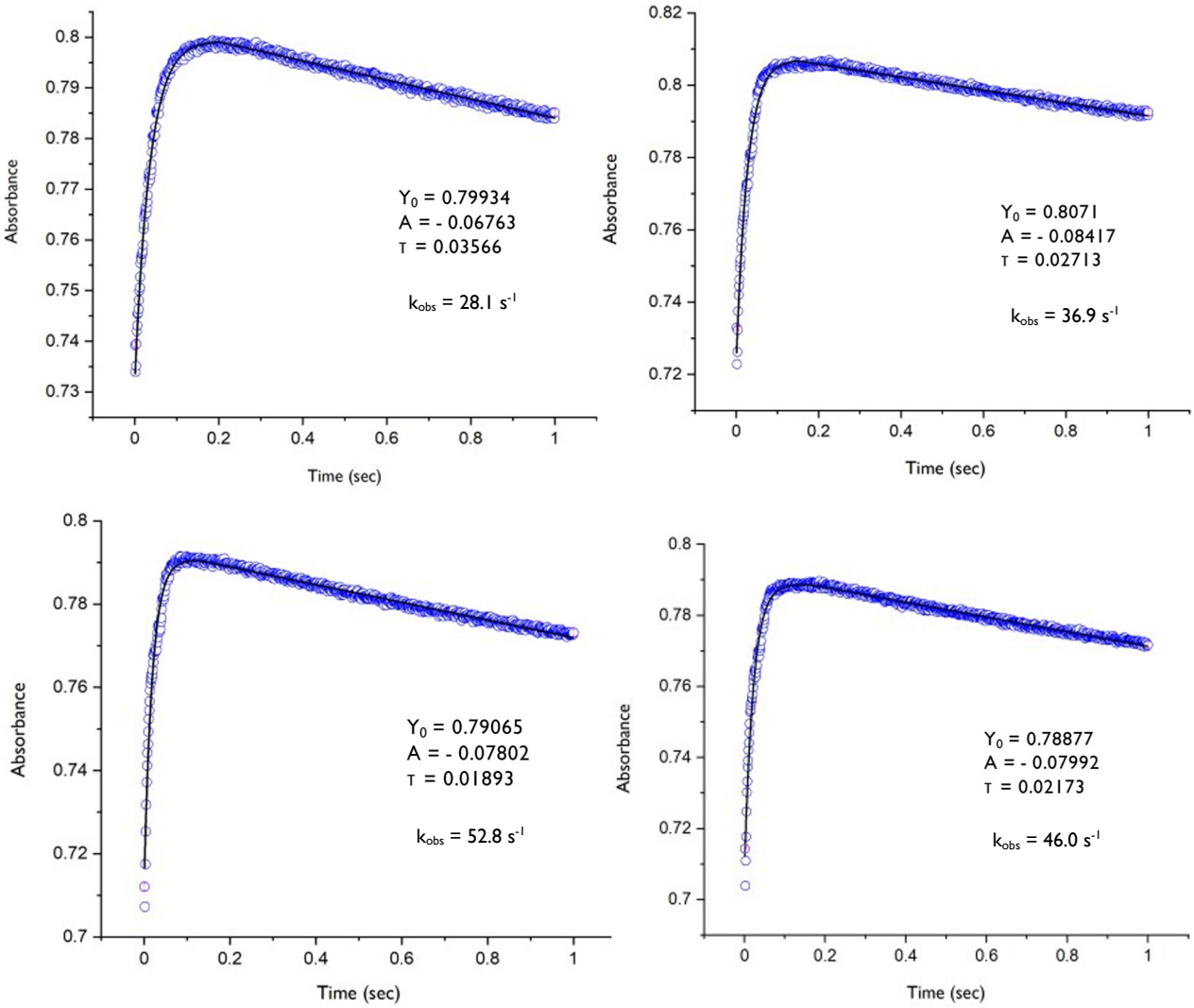

Figure S15. Detection of monocyclic product after sequential mix reaction of OxyB with *m*CPBA and 7mer-CoA. The reaction was conducted as described in Fig. S14. Subsequently, the material in the stop syringe was collected and subjected to HPLC-Qtof-MS. The extracted ion chromatograms show presence of substrate (left, black trace) and the monocyclic product (left, green trace). For the HR-MS profiles, we have focused on substrate (top, right) or zoomed in to focus on product (bottom, right). Both substrate and product were also subjected to high-resolution tandem-MS (Table S1), which provide further confirmation for the presence of substrate and monocyclic product.

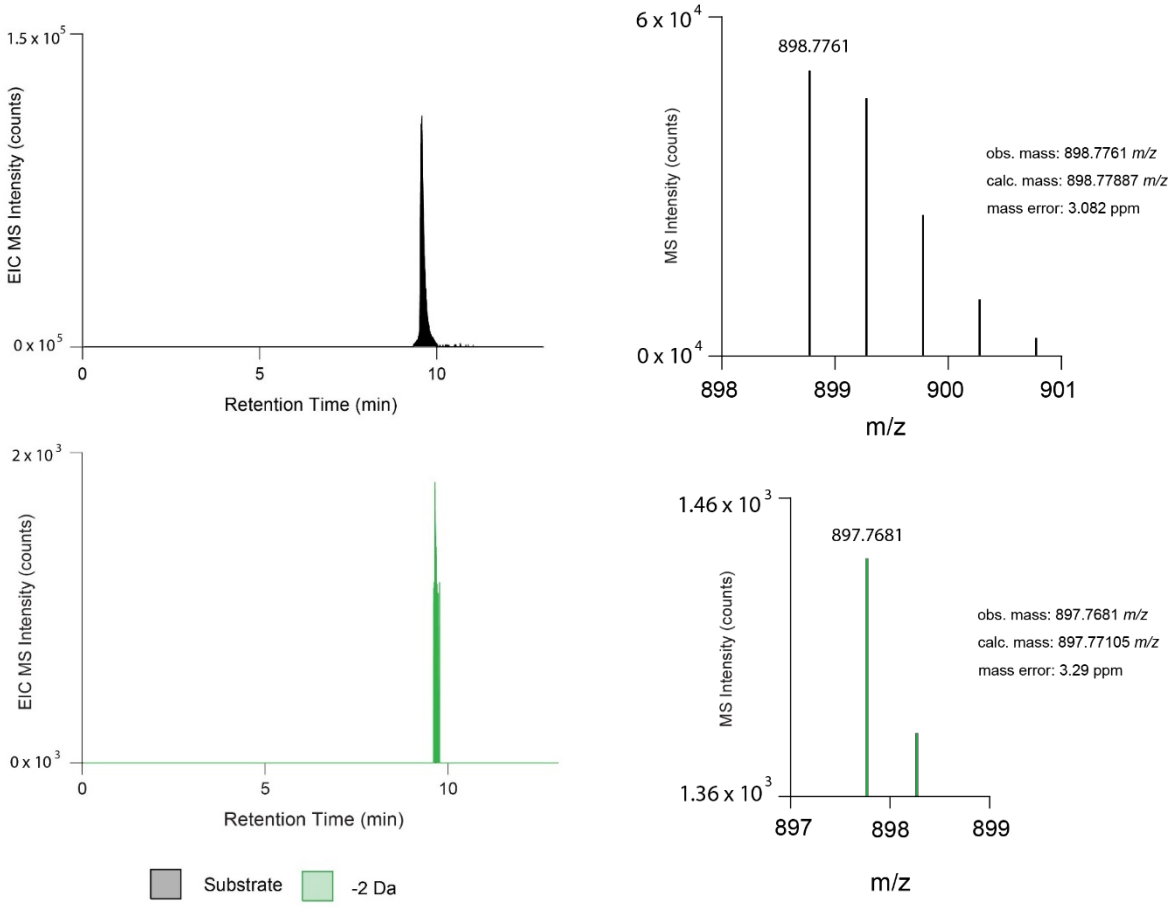

Table S1. High-resolution tandem mass spectrometric analysis of remaining substrate from the OxyB reaction. Samples were generated in a sequential mix SF UV/Vis set after mixing OxyB with *m*CPBA to generate cpd-I, followed by mixing this intermediate with the vancomycin 7mer-CoA peptide. The contents of the stop syringe were then quenched and subjected to analysis. Observed fragment ions and derived sequences are shown for each substrate (below) and product (Table S2, page S19). Fragments are mapped onto the structure below the table.

Ion	Calculated *m/z*	Observed *m/z*	Δppm	Sequence
b_2^{+1}	291.17032	291.1721	6.1	MeLeu-Tyr
b_3^{+1}	405.21325	405.2142	2.3	MeLeu-Tyr-Asn
b_4^{+1}	554.26092	554.2657	8.6	MeLeu-Tyr-Asn-Hpg
b_5^{+1}	703.30860	703.3042	6.2	MeLeu-Tyr-Asn-Hpg-Hpg
b_6^{+1}	866.37193	866.3755	4.1	MeLeu-Tyr-Asn-Hpg-Hpg-Tyr
b_7^{+1}	1029.43526	1029.4374	2.1	MeLeu-Tyr-Asn-Hpg-Hpg-Tyr-Tyr
M+H-ADP^{+1}	1289.55472	1289.5599	4.0	MeLeu-Tyr-Asn-Hpg-Hpg-Tyr-Tyr
M+H-AMP^{+1}	1369.52105	1369.5261	3.7	MeLeu-Tyr-Asn-Hpg-Hpg-Tyr-Tyr

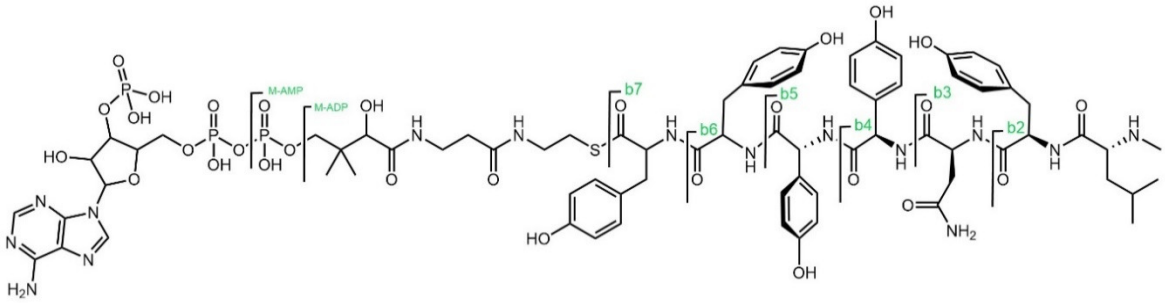

Table S2. High-resolution tandem mass spectrometric analysis of product from the OxyB reaction. See description of Table S1. Observed fragment ions and derived sequences are shown for the product, which are mapped onto the structure below the table. Notably, the b4 and b5 ions are not observed in the product, and the b6 ion is 2 mass units lighter as would be expected for the product containing the macrocycle.[2,4]

Ion	Calc m/z	Obs m/z	Δppm	Sequence
b_2^{+1}	291.17032	291.1677	9.0	MeLeu-Tyr
b_3^{+1}	405.21325	405.2160	6.8	MeLeu-Tyr-Asn
b_6^{+1}	864.35628	864.3505	6.7	MeLeu-Tyr-Asn-Hpg-Hpg-Tyr
b_7^{+1}	1027.41961	1027.4175	2.1	MeLeu-Tyr-Asn-Hpg-Hpg-Tyr-Tyr
M+H-ADP^{+1}	1287.53907	1287.5398	0.6	MeLeu-Tyr-Asn-Hpg-Hpg-Tyr-Tyr
M+H-AMP^{+1}	1367.50540	1367.5058	0.3	MeLeu-Tyr-Asn-Hpg-Hpg-Tyr-Tyr

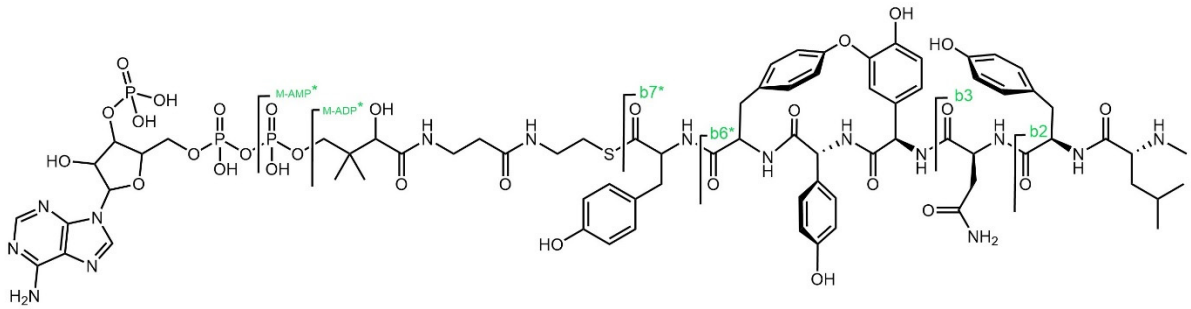

Supporting References

1. Zerbe, K., Pylypenko, O., Vitali, F., Zhang, W., Rouset, S., Heck, M., Vrijbloed, J. W., Bischoff, D., Bister, D., Süssmuth, R. D., Pelzer, D., Wohlleben, W., Robinson, J. A., Schlichting, I. Crystal structure of OxyB, a cytochrome P450 implicated in an oxidative phenol coupling reaction during vancomycin biosynthesis. *J. Biol. Chem.* **2002**, *277*, 47476–47485.

2. Forneris, C. F.; Ozturk, S.; Gibson, M. I.; Sorensen, E. J.; Seyedsayamdost, M. R. In Vitro Reconstitution of OxyA Enzymatic Activity Clarifies Late Steps in Vancomycin Biosynthesis. *ACS Chem. Biol.* **2017**, *12*, 2248–2253.

3. Rittle, J.; Younker, J. M.; Green, M. T. Cytochrome P450: The Active Oxidant and Its Spectrum. *Inorg. Chem.* **2010**, *49*, 3610–3617.

4. Forneris, C. F.; Nguy, A. K. L.; Seyedsayamdost, M. R. Mapping and Exploiting the Promiscuity of OxyB Toward the Biocatalytic Production of Vancomycin Aglycone Variants. *ACS Catal.* **2020**, *10*, 9287–9298.